

# Urolithin A induces mitophagy and prolongs lifespan in *C. elegans* and increases muscle function in rodents

Dongryeol Ryu<sup>1,5</sup>, Laurent Mouchiroud<sup>1,5</sup>, Pénélope A Andreux<sup>1,2,5</sup>, Elena Katsyuba<sup>1</sup>, Norman Moullan<sup>1</sup>, Amandine A Nicolet-dit-Félix<sup>1</sup>, Evan G Williams<sup>1</sup>, Pooja Jha<sup>1</sup>, Giuseppe Lo Sasso<sup>1</sup>, Damien Huzard<sup>3</sup>, Patrick Aebischer<sup>4</sup>, Carmen Sandi<sup>3</sup>, Chris Rinsch<sup>2</sup> & Johan Auwerx<sup>1,7</sup>

The biological effects of urolithins remain poorly characterized, despite wide-spread human exposure via the dietary consumption of their metabolic precursors, the ellagitannins, which are found in the pomegranate fruit, as well as in nuts and berries. We found that urolithin A (UA) is a previously unknown, first-in-class natural compound that induces mitophagy both *in vitro* and *in vivo* following oral consumption. In *C. elegans*, UA prevented the accumulation of dysfunctional mitochondria with age and extended lifespan. Likewise, UA prolonged normal activity during aging in *C. elegans*, including mobility and pharyngeal pumping, while maintaining mitochondrial respiratory capacity. These effects translated to rodents, where UA improved exercise capacity in two different mouse models of age-related decline of muscle function, as well as in young rats. Our findings highlight the health benefits of urolithin A and its potential application in strategies to improve mitochondrial and muscle function.

The evolution of society from its hunter-gatherer origins to its present form has come with a marked shift in dietary behavior. Berries, nuts, acorns and tree leaves, all found in the wild, serve as an important dietary staple of animals today and humans long ago<sup>1</sup>. Natural compounds known as ellagitannins (ETs) are a common denominator uniting, from a phytochemistry viewpoint, many of these ancestral foods<sup>2</sup>. For humans, the pomegranate fruit is a prominent source of ellagitannins in general and of punicalagin in particular<sup>3</sup>. ETs are hydrolyzed in the gut to release ellagic acid (EA), which is further processed by the microflora into urolithins through the loss of one of its two lactones and by successive removal of hydroxyl groups<sup>4</sup> (Fig. 1a). In the species investigated to date (including humans), urolithin A (UA), urolithin B (UB), urolithin C (UC) and urolithin D (UD) are the redundant measurable metabolites that are thought to be the end-products of both ETs and EA<sup>4,5</sup>.

Until now, there has not been an in-depth investigation into the mechanism of action of urolithins and their benefits following chronic administration. Most studies exploring urolithins *in vivo* have focused on their metabolism by administering a source of ETs (either mixed or pure) and subsequently monitoring their conversion into either EA or urolithins<sup>5–8</sup>. Notably, it has been observed that intestinal biotransformation of EA into urolithins is heterogeneous across individuals, with individuals showing high or low conversion rates, as well as those who do not convert at all<sup>9</sup>. A few studies have documented biological effects of urolithins *in vitro*, including antiproliferation in cancer cell models<sup>10</sup>, anti-inflammation<sup>11</sup> and benefits on lipid metabolism<sup>12</sup>, although a clear biological pathway has not yet been described.

Here we characterized the biological effects of urolithins, and UA in particular, using *C. elegans* as a model organism. We subsequently investigated the activity of UA in mammalian cells and explored their health benefits in rodents.

## RESULTS

### Urolithins extend lifespan and improve fitness in *C. elegans*

We found that feeding worms from eggs until death with UA, UB, UC or UD at a standard concentration of 50  $\mu$ M extended lifespan by 45.4, 36.6, 36.0 and 19.0%, respectively, as compared to the vehicle-treated population (Fig. 1b). In contrast, treatment with EA at the same concentration had no effect on lifespan (Fig. 1b). Thus, we decided to continue with a deeper investigation of urolithins, and we focused on UA, as it is the most prevalent EA-derived metabolite observed in humans<sup>5,9</sup>. We found a clear dose-response effect on lifespan when UA concentrations were increased from 10 to 50  $\mu$ M (Fig. 1c). At 50  $\mu$ M, UA significantly delayed the mortality observed at advanced ages (Fig. 1d).

Similar to other organisms, fasting is one of the well-known mechanisms by which worm lifespan can be extended<sup>13</sup>. Fasting can be induced if a compound affects bacterial growth, thereby reducing the amount of food available or modifying key nutrient amounts<sup>14</sup>, or acts as repellent for the worms and prevents food intake. To test the first possibility, we measured the effect of UA on bacterial metabolism by measuring the growth of two *Escherichia coli* strains, OP50 and HT115, after treatment with UA. We found that UA had a very modest effect on the growth of these two strains (Supplementary Fig. 1a,b).

<sup>1</sup>Laboratory for Integrative and Systems Physiology, Interfaculty Institute of Bioengineering, Ecole Polytechnique Fédérale de Lausanne, Lausanne, Switzerland.

<sup>2</sup>Amazentis SA, Ecole Polytechnique Fédérale de Lausanne Innovation Park, Batiment C, Lausanne, Switzerland. <sup>3</sup>Laboratory of Behavioral Genetics, Brain Mind Institute, School of Life Sciences, Ecole Polytechnique Fédérale de Lausanne, Lausanne, Switzerland. <sup>4</sup>Brain Mind Institute, Ecole Polytechnique Fédérale de Lausanne, Lausanne, Switzerland. <sup>5</sup>These authors contributed equally to this work. Correspondence should be addressed to J.A. (admin.auwerx@epfl.ch) or C.R. (contact@amazentis.com).

Received 6 January; accepted 25 May; published online XX XX 2016; doi:10.1038/nm.4132

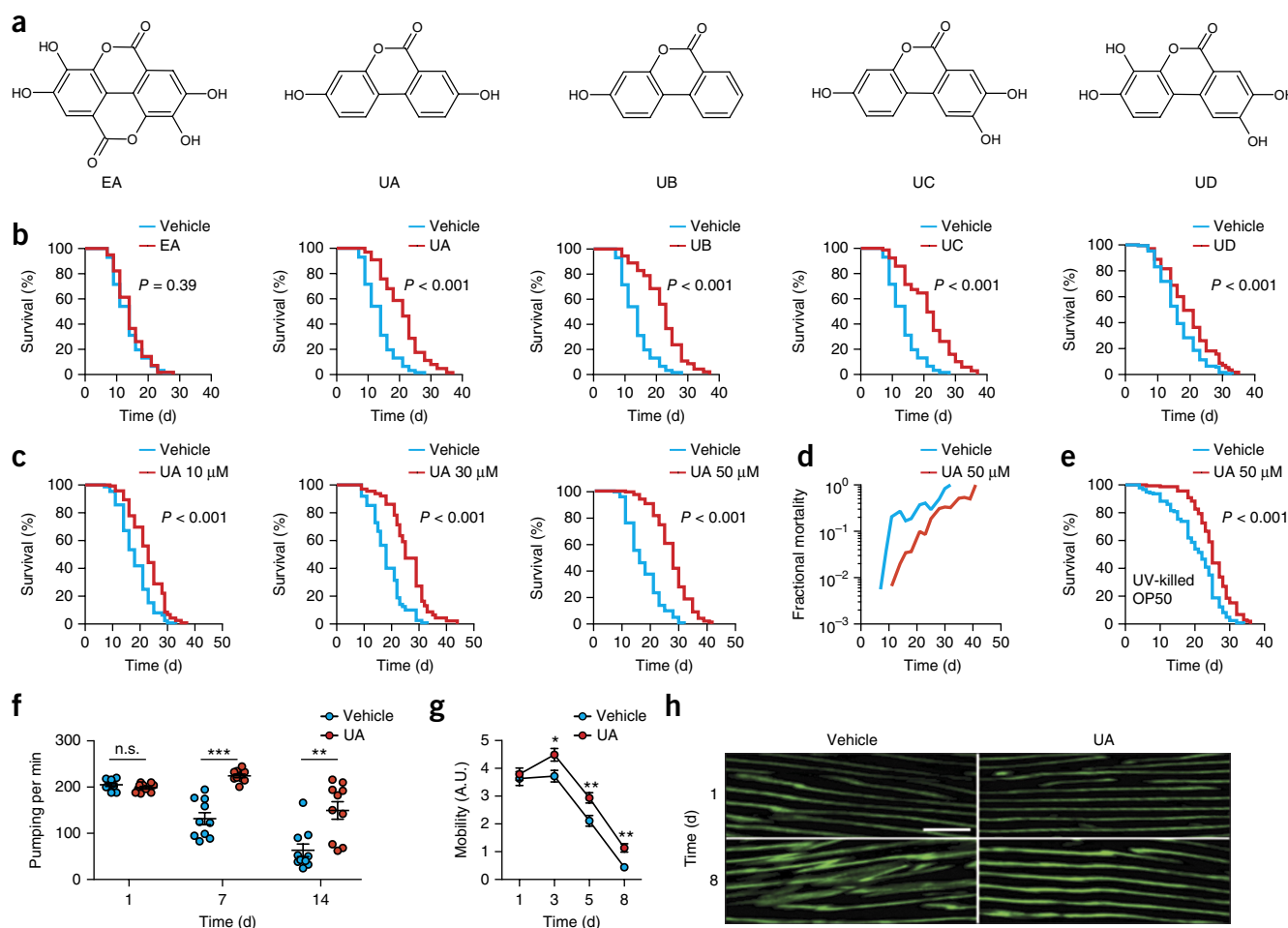


**Figure 1** UA improves fitness and extends lifespan. (a) Chemical structures of EA and its derived metabolites UA, UB, UC and UD. (b) Lifespan of worms treated with 50  $\mu$ M EA, UA, UB, UC or UD, or with vehicle (1% DMSO). (c) Lifespan of worms treated with 10, 30 or 50  $\mu$ M UA, or the corresponding concentration of vehicle. (d) Mortality rate in worms treated with 50  $\mu$ M UA or vehicle. (e) Lifespan of worms maintained on UV-killed OP50 bacteria treated with 50  $\mu$ M UA or vehicle. For b,c,e,  $P$  values represent comparison with vehicle calculated using log rank test. (f) Pharyngeal pumping at days 1, 7 and 14 of adulthood in worms treated with 50  $\mu$ M UA or vehicle ( $n = 10$ ). Values are mean  $\pm$  s.e.m. n.s., not significant; \*\* $P \leq 0.01$ , \*\*\* $P \leq 0.001$  by unpaired  $t$  test. (g) Mobility of worms in arbitrary units (A.U.) at days 1, 3, 5 and 8 of adulthood in worms treated with 50  $\mu$ M UA or vehicle ( $n = 10$ ). Values are mean  $\pm$  s.e.m. \* $P \leq 0.05$ , \*\* $P \leq 0.01$ ; by two-way analysis of variance (ANOVA) followed by Bonferroni post-tests. (h) Representative images ( $n = 5$  images per group) of muscle morphology at days 1 and 8 of adulthood of  $p_{myo-3}::MYO-3::GFP$  worms treated with 50  $\mu$ M UA or vehicle. Scale bar, 8  $\mu$ m. Data are representative of at least two independent experiments. See also **Supplementary Figures 1–3** and **Supplementary Tables 1** and **2**.

In addition, UA extended lifespan in worms fed with both bacterial strains, and we observed a greater effect in worms fed with OP50 than in those fed with HT115 (**Supplementary Fig. 1c,d**). With regards to the second possibility, we found that worms did not avoid bacteria treated with UA (**Supplementary Fig. 1e,f**). These results indicate that UA does not extend lifespan by affecting the amount of bacteria available, bacterial metabolism or food intake. Notably, UA also increased worm lifespan as compared with untreated controls when fed bacteria killed by UV radiation (**Fig. 1e**). Altogether, these data demonstrate that UA-mediated extension of lifespan occurs by a direct effect on *C. elegans* rather than indirectly through the bacteria.

We next evaluated the effect of UA on worm activity by assessing the pharyngeal pumping rate and mobility, both of which were robustly improved by UA treatment during aging as compared with vehicle (**Fig. 1f,g**). This improvement in the UA-treated group correlated with a better maintenance of the muscle fiber organization (**Fig. 1h**). Similar effects on activity were observed with UB,

whereas EA, UC and UD showed mild-to-no benefit during aging (**Supplementary Fig. 2a,b**).

Lifespan extension is often associated with adverse effects during the larval stage by reducing fertility or delaying development<sup>15</sup>. UA treatment did not interfere with the development of progeny, although it was associated with slightly greater worm fertility compared with the vehicle-treated group (**Supplementary Fig. 2c,d**). In fact, UA was observed to act during adulthood, as lifespan extension by UA did not require a life-long exposure, and treatment for short periods of time during adulthood was sufficient to prolong life compared with vehicle treatment (**Supplementary Fig. 3a,b**).

### UA requires mitochondrial function to extend lifespan

We next dissected the longevity pathways required for the lifespan extension induced by UA by testing its effects in prototypical mutants for insulin/IGF-1 signaling<sup>16</sup>, caloric restriction<sup>17</sup> and mitochondrial dysfunction<sup>17–21</sup>. Both *daf-16* (insulin/IGF-1) and *eat-2* (caloric restriction)

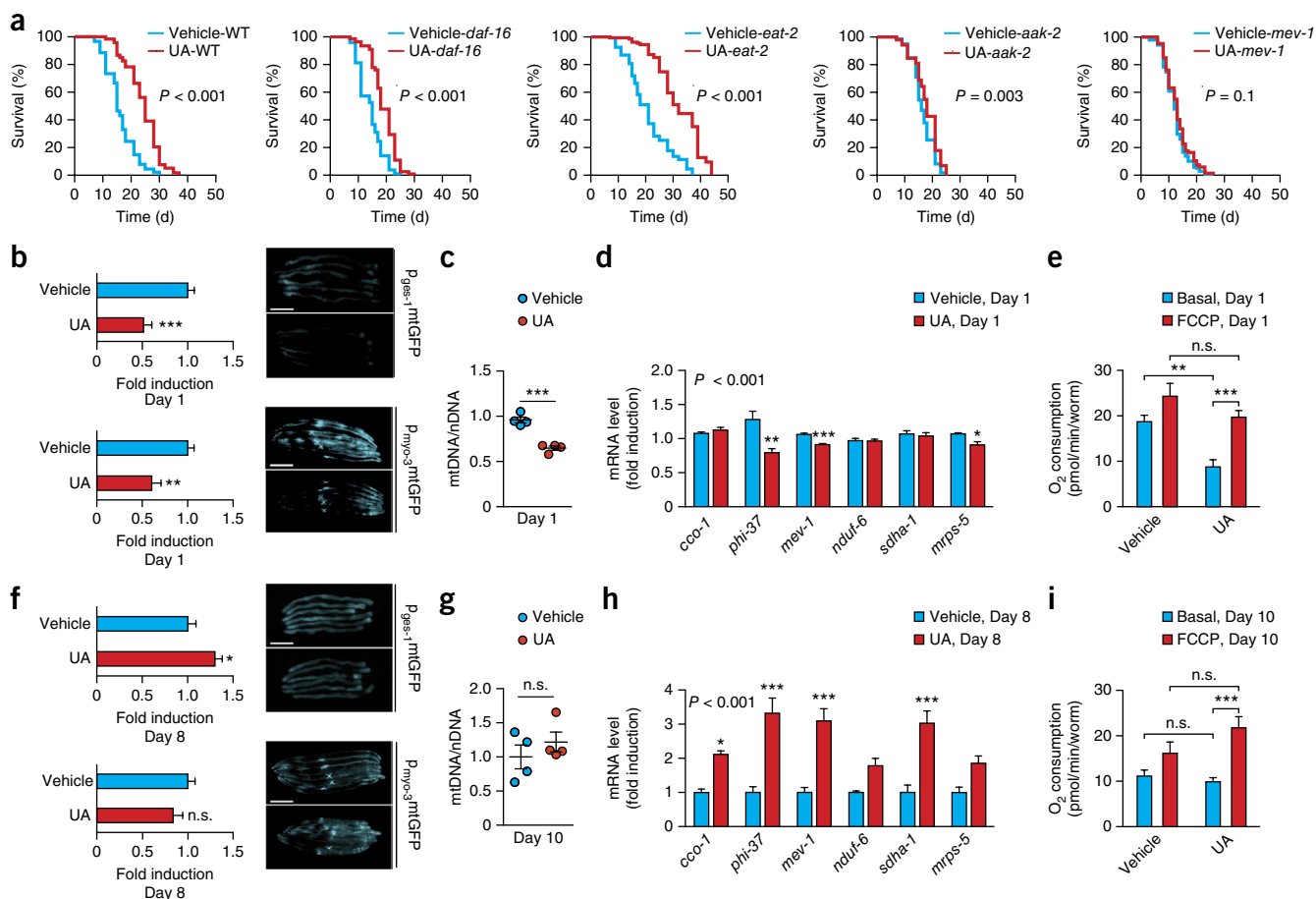


**Figure 2** UA alters mitochondrial functions in *C. elegans*. **(a)** Lifespan of wild-type, *daf-16(mu86)*, *eat-2(ad465)*, *aak-2(ok524)* and *mev-1(kn1)* mutants treated with UA or vehicle. *P* values compared with vehicle calculated using log-rank test. **(b)** Representative images (left, *n* = 3) and GFP quantification (right, *n* = 8) of mitochondrial content at day 1 of adulthood in intestinal (*p<sub>ges-1</sub>::mtGFP*; top) and muscle (*p<sub>myo-3</sub>::mtGFP*; bottom) mito::GFP reporter strains treated with UA or vehicle. **(c)** mtDNA/nDNA ratio at day 1 of adulthood in wild-type worms treated with UA or vehicle (*n* = 4). For **b,c**, \*\**P* ≤ 0.01, \*\*\**P* ≤ 0.001; by unpaired *t* test. **(d)** Gene expression at day 1 of adulthood in wild-type worms treated with UA or vehicle (*n* = 5). \**P* ≤ 0.05, \*\**P* ≤ 0.01, \*\*\**P* ≤ 0.001; by one-way ANOVA. **(e)** Respiration at basal level and after short-term incubation with 10 μM FCCP on day 1 of adulthood in wild-type worms treated with UA or vehicle (*n* = 5). \*\**P* ≤ 0.01, \*\*\**P* ≤ 0.001; n.s., not significant; by two-way ANOVA followed by Bonferroni post-tests. **(f)** Representative images (left, *n* = 3) and GFP quantification (right, *n* = 8) of mitochondrial content at day 8 of adulthood in intestinal (*p<sub>ges-1</sub>::mtGFP*; top) and muscle (*p<sub>myo-3</sub>::mtGFP*; bottom) mito::GFP reporter strains treated with UA or vehicle (*n* = 8). **(g)** mtDNA/nDNA ratio on day 10 of adulthood in wild-type worms treated with UA or vehicle (*n* = 4). For **f,g**, \**P* ≤ 0.05; n.s., not significant; by unpaired *t*-test. **(h)** Gene expression on day 8 of adulthood in wild-type worms treated with UA or vehicle (*n* = 5). \**P* ≤ 0.05, \*\*\**P* ≤ 0.001; by one-way ANOVA. **(i)** Respiration at basal level and after short-term incubation with 10 μM FCCP on day 10 of adulthood in wild-type worms treated with UA or vehicle (*n* = 5). \*\*\**P* ≤ 0.001; n.s., not significant; by two-way ANOVA followed by Bonferroni post-tests. For **b,f**, scale bars, 250 μm. UA was used at 50 μM. Values are mean ± s.e.m. Data are representative of at least two independent experiments. See also **Supplementary Figure 3** and **Supplementary Table 1**.

mutant worms had an extended mean lifespan with UA treatment as compared with their respective vehicle-treated groups (**Fig. 2a**). In contrast, life extension by UA was partially dependent on AMP-activated protein kinase (AMPK), as there was only a mild increase in lifespan in *aak-2* (AMPK homolog) mutants treated with UA versus vehicle (**Fig. 2a**). However, the effect of UA on lifespan was dependent on mitochondrial function, as the improvement was entirely suppressed in *mev-1* (mitochondrial succinate dehydrogenase complex subunit C, SDHC) mutants (**Fig. 2a**).

To further understand the effects of UA on aging, we monitored young (day 1) and old (days 8–10) worms that were treated with UA starting from the egg stage for both mitochondrial content and function. In young worms, UA treatment resulted in lower mitochondrial content in intestinal and muscle cells compared with vehicle treatment (**Fig. 2b**). These observations were confirmed at the molecular level

by a lower mitochondrial DNA to nuclear DNA (mtDNA/nDNA) ratio in whole worms (**Fig. 2c**), as well as by a lower expression of some respiratory chain subunits at the mRNA and protein levels in the UA-treated versus vehicle-treated worms (**Fig. 2d** and **Supplementary Fig. 3c**). We also observed, as expected, a lower degree of basal mitochondrial respiration at day 1 in UA-treated versus vehicle-treated worms (**Fig. 2e**). However, we found that mitochondrial function was not impaired in the UA-treated group, as exposure to the uncoupling agent carbonyl cyanide-*p*-trifluoromethoxyphenylhydrazone (FCCP) induced approximately twofold greater respiration than basal levels (**Fig. 2e**). Furthermore, UA treatment was associated with significantly lower ATP content at day 1 than vehicle treatment (**Supplementary Fig. 3d**). Unlike young worms, old worms exposed to UA had mitochondria numbers comparable to or higher than those of vehicle-treated controls (**Fig. 2f,g**). Aged worms treated with UA had higher

Q4

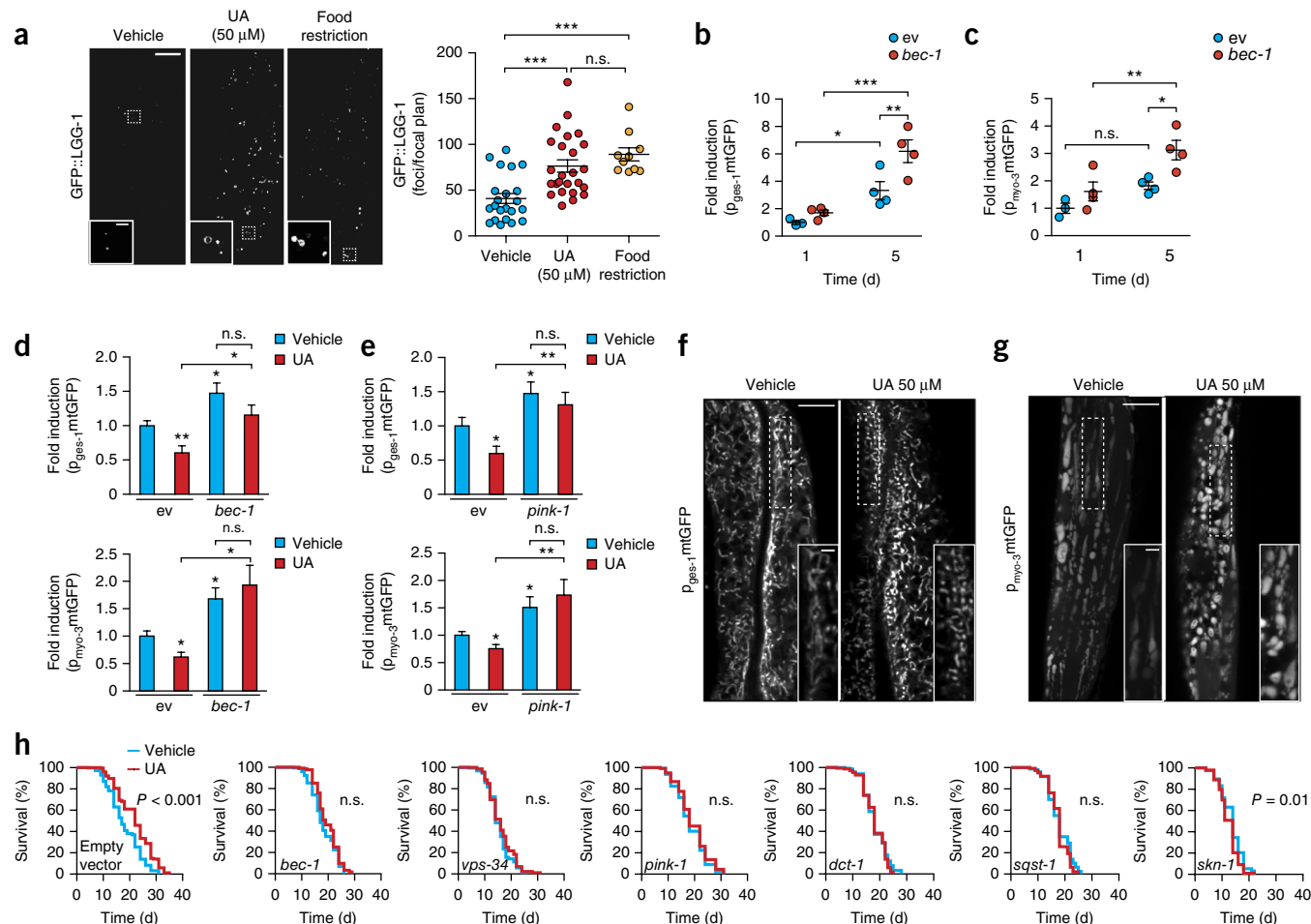


**Figure 3** Mitophagy is required for UA-mediated longevity phenotype. **(a)** Representative images (left,  $n = 10$ –25 images per group) and quantification of foci (right) in GFP::LGG-1 worms on day 2 of adulthood after treatment with vehicle, 50  $\mu$ M UA or food restriction. Results were pooled from three independent experiments. \*\*\* $P \leq 0.001$ ; n.s., not significant by one-way ANOVA. Insets show a higher magnification of the image in the dashed rectangle. Scale bars represent 8  $\mu$ m (main) and 1  $\mu$ m (inset). **(b,c)** Mitochondrial content on day 1 and 5 of adulthood in intestinal ( $p_{ges-1}$ mtGFP; **b**) and muscle ( $p_{myo-3}$ mtGFP; **c**) mito::GFP reporter strains fed with ev ( $n = 3$ ) or *bec-1* ( $n = 4$ ) RNAi. \* $P \leq 0.05$ ; \*\* $P \leq 0.01$ ; \*\*\* $P \leq 0.001$ ; n.s., not significant by two-way ANOVA followed by Bonferroni post-tests. **(d,e)** Mitochondrial content on day 1 of adulthood in intestinal ( $p_{ges-1}$ mtGFP; top) and muscle ( $p_{myo-3}$ mtGFP; bottom) mito::GFP reporter strains fed with ev, *bec-1* or *pink-1* RNAi and treated with UA or vehicle ( $n = 8$ ). \* $P \leq 0.05$ ; \*\* $P \leq 0.01$ ; n.s., not significant by unpaired  $t$  test. **(f,g)** Representative images ( $n = 8$  images per group) of intestinal ( $p_{ges-1}$ mtGFP; **f**) and muscle ( $p_{myo-3}$ mtGFP; **g**) mito::GFP reporter strains on day 1 of adulthood after treatment with UA or vehicle. Insets show a higher magnification of the image in the dashed rectangle. Scale bars represent 8  $\mu$ m (main) and 2  $\mu$ m (inset). **(h)** Lifespan of worms fed with *bec-1*, *vps-34*, *pink-1*, *dct-1*, *sqst-1* and *skn-1* RNAi and treated with UA or vehicle.  $P$  values compared with vehicle calculated using log-rank test. n.s., not significant. Data are representative of at least two independent experiments. Values are mean  $\pm$  s.e.m. UA was used at 50  $\mu$ M. ev, scrambled RNAi. See also **Supplementary Figures 4 and 5** and **Supplementary Table 1**.

transcript levels of respiratory chain subunits (Fig. 2h), ATP content was stable (Supplementary Fig. 3e), whereas maximal respiration capacity was greater (Fig. 2i), compared with vehicle-treated worms. Thus, after initially lower mitochondria content following short-term UA treatment, long-term UA exposure results in greater mitochondria content than vehicle exposure, suggesting that UA treatment activates mitochondria biogenesis in older worms.

We also ruled out several stress pathways as potential causes for the lower mitochondrial content and function after short-term UA exposure compared with vehicle. Specifically, as with vehicle treatment, UA had no effect on the mitochondrial unfolded protein response (*hsp-6::gfp*), heat shock stress (*hsp-16.2::gfp*), endoplasmic reticulum (ER) stress (*hsp-4::gfp*) or oxidative stress (*gst-4::gfp*), as measured by induction of appropriate reporter constructs in transgenic worms (Supplementary Fig. 3f).

### UA exerts its beneficial effects through the induction of mitophagy

A possible explanation for the lower mitochondrial content in young worms treated with UA versus vehicle is that UA might induce the selective autophagy of mitochondria (mitophagy). To test this hypothesis, we monitored autophagy in a reporter strain expressing the *C. elegans* microtubule-associated protein 1 light chain 3 beta (LC3B) autophagosome protein LGG-1 fused with GFP<sup>22</sup>. We found that UA induced the formation of GFP::LGG-1-positive punctae in a fashion comparable to food restriction, an established inducer of autophagy in *C. elegans*<sup>23</sup> (Fig. 3a). This change in autophagy was confirmed at the transcriptional level, where expression of both autophagy and mitophagy genes were greater in young worms, and to a lesser extent in old worms, in UA-treated versus vehicle-treated worms (Supplementary Fig. 4a). Silencing the homolog of Beclin1 (*bec-1*)—a primary regulator of autophagy<sup>24</sup>—by RNA interference



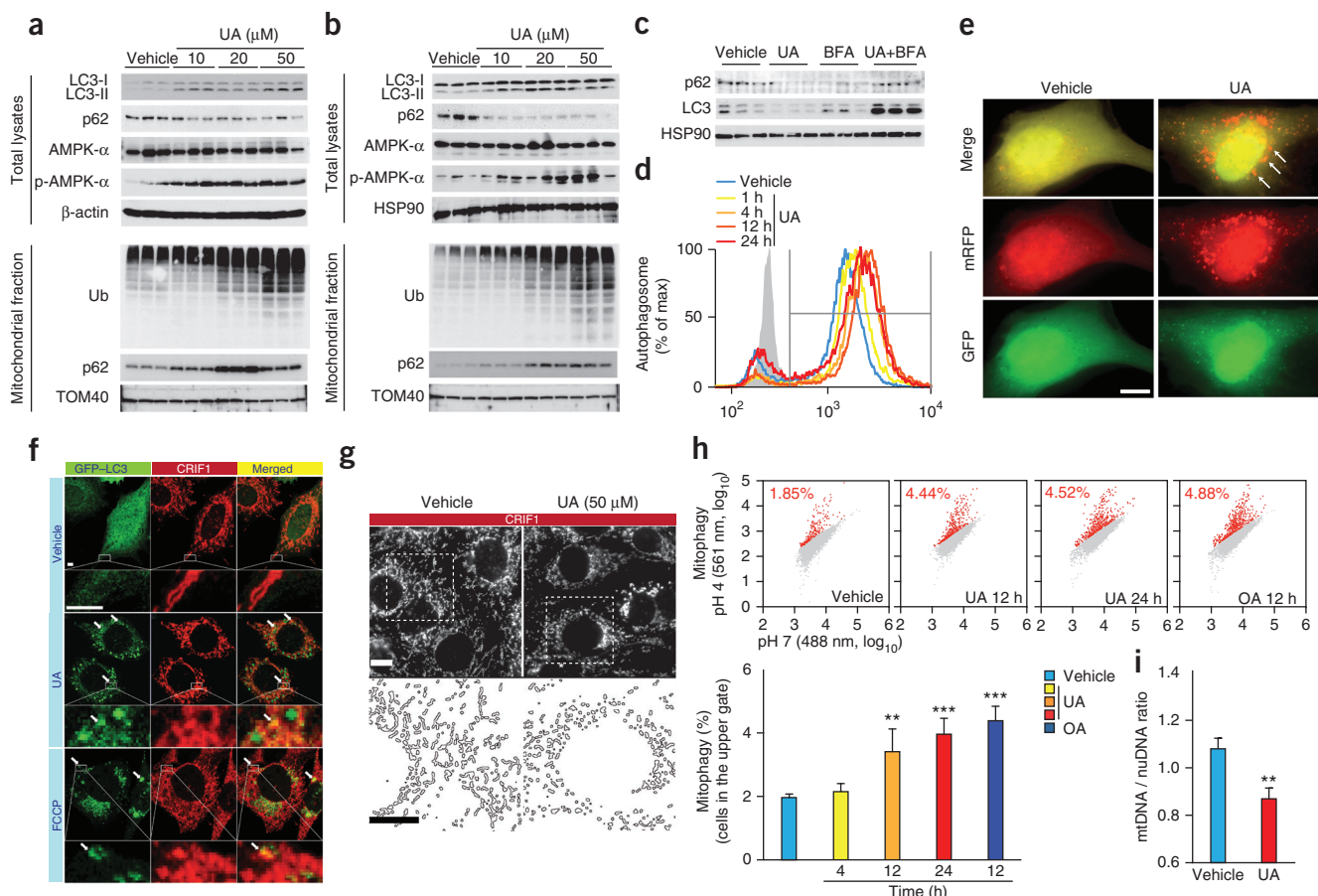


**Figure 4** UA induces mitophagy in muscle and intestinal mouse cell lines. (**a,b**) Western blots of total lysate (top) or mitochondrial fraction (bottom) of C2C12 myoblasts (**a**,  $n = 3$  biological replicates) and Mode K cells (**b**,  $n = 3$  biological replicates) treated with 10, 20 or 50  $\mu$ M UA or vehicle (0.1% DMSO) for 20 h. (**c**) Western blot of C2C12 myoblasts treated with UA or vehicle for 24 h and/or with bafilomycin A (BFA), an inhibitor of lysosomal acidification, at 10 nM for 4 h ( $n = 3$  biological replicates). (**d**) Quantification of the fluorescence intensity of the CytoD dye, a probe that accumulates in endogenous autophagosomes, by FACS in C2C12 myoblasts ( $n = 4$ ). (**e**) Representative images ( $n = 3$  images per group) of C2C12 myoblasts treated with UA or vehicle for 24 h and transfected with mRFP-GFP-LC3B construct to visualize autolysosomes (white arrows). Scale bar, 10  $\mu$ m. (**f,g**) Representative images ( $n = 3$  images per group) of Mode-K cells overexpressing GFP-LC3 and stained for mitochondria with an antibody to CRIF1, an essential component of the large subunit of mammalian mitochondrial ribosome<sup>53,54</sup>. (**f**) Scale bar represents 25  $\mu$ m. Insets show higher magnification of the image. (**g**) CRIF1 fluorescence only. Scale bar represents 10  $\mu$ m. Insets show higher magnification of the image. (**h**) Quantification of pHRed-positive populations by FACS (red dots and values in red, upper) in C2C12 myoblasts transfected with mitochondrial pHRed and treated with vehicle, UA or OA (1  $\mu$ g/ml oligomycin + 1.25  $\mu$ M antimycin A) ( $n = 4$ ). Values are mean  $\pm$  s.e.m. \*\* $P \leq 0.01$ ; \*\*\* $P \leq 0.001$  for comparison with vehicle after one-way ANOVA. (**i**) mtDNA/nuDNA ratio in C2C12 myoblasts treated with UA or vehicle for 24 h ( $n = 6$ ). Values are mean  $\pm$  s.e.m. \*\* $P \leq 0.01$  after Student's *t*-test. Data and images are representative of two (**a,b,i**) or four (**c–h**) independent experiments. All treatments were made with 50  $\mu$ M UA unless stated otherwise. See also **Supplementary Figure 6**.

**Q5** (RNAi) led to a higher mitochondrial content in the muscle and intestine at day 5 compared with control worms (**Fig. 3b,c**), similar to what has been reported<sup>25</sup>. Consistent with this, we found that mitochondrial elimination was completely lost in UA-treated worms compared with vehicle treatment following the knockdown of *bec-1* or the autophagosome adaptor sequestosome/p62 (*sqst-1*) at day 1 (**Fig. 3d** and **Supplementary Fig. 4b**). Furthermore, when we silenced mitophagy using RNAi against either the mitochondrial phosphatase and tensin (PTEN)-induced kinase 1 (*pink-1*) or the BCL2/adenovirus E1B interacting protein 3 (BNIP3) homolog (*dct-1*), we observed the same effects as when *bec-1* and *sqst-1* were silenced (**Fig. 3e** and **Supplementary Fig. 4c**). The greater mobility induced by UA compared with vehicle at day 8 was also lost in the absence of *bec-1* and *pink-1* (**Supplementary Fig. 4d,e**). Furthermore, when we inhibited mitophagy genes by RNAi (*pink-1*) or mutation (*pdr-1*, the worm homolog of parkin RBR E3 ubiquitin protein ligase PARK2), the lower

oxygen consumption rate (OCR) measured in UA-treated compared with vehicle-treated worms was abolished (**Supplementary Fig. 4f,g**). On a structural level, we also found that the mitochondrial network in both intestine and muscle was more fragmented following UA treatment than vehicle treatment (**Fig. 3f,g** and **Supplementary Fig. 4h,i**), consistent with the fact that mitophagy and mitochondrial fission are intimately linked<sup>26–28</sup>. This fragmentation was accompanied by lower mRNA levels of *fzo-1* and *opa-1*, two major components of the mitochondrial fusion machinery, in the UA-treated versus vehicle-treated groups (**Supplementary Fig. 4j**). Likewise, we found that lifespan extension following UA exposure was dependent on the expression of the autophagy genes *bec-1*, *sqst-1* and *vps-34* (class III PI3 kinase homolog), and the mitophagy genes *pink-1*, *dct-1* and *skn-1* (nuclear factor, erythroid derived 2, like 2 (Nrf2) homolog), the latter of which was recently identified as a transcription factor regulating mitochondrial biogenesis and mitophagy gene expression<sup>25</sup> (**Fig. 3h**).

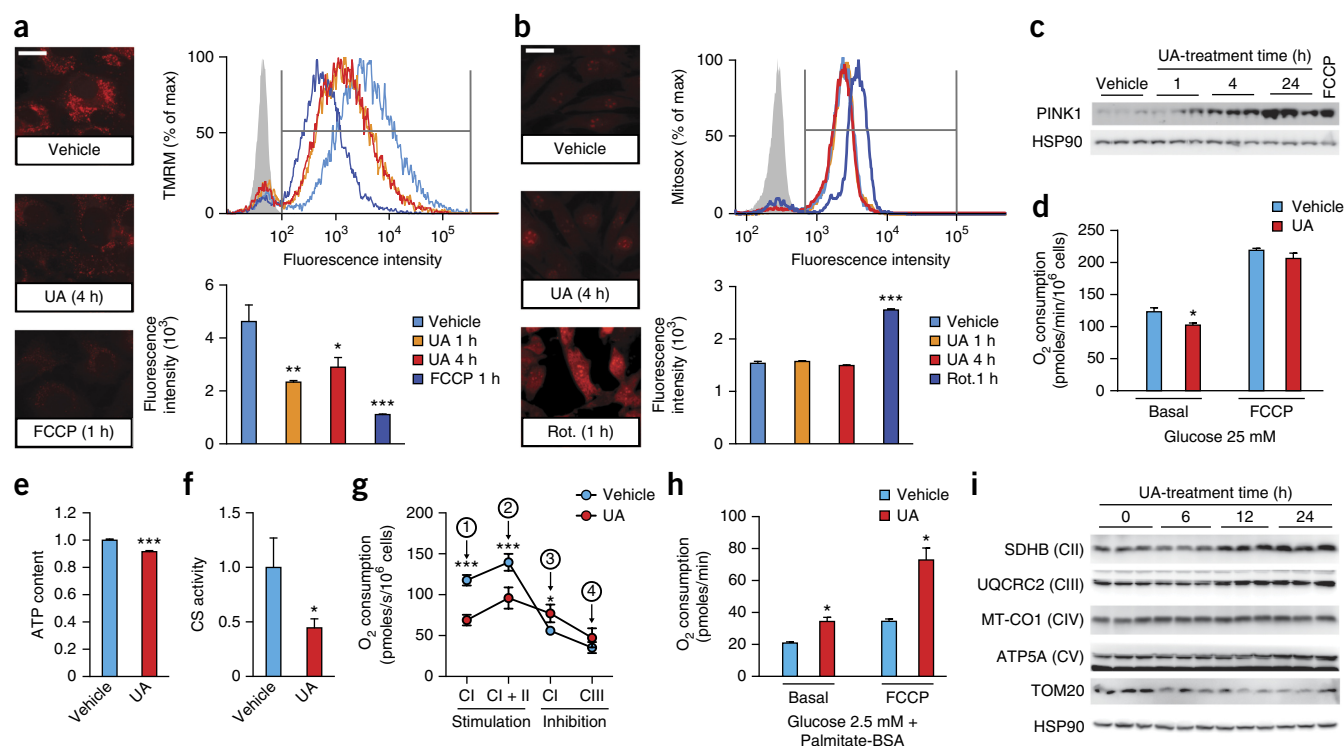


**Figure 5** UA shifts mitochondria from CI- to CII-driven respiration. **(a)** Representative images ( $n = 5$ –10 images per group) and quantification of TMRM fluorescence by FACS in C2C12 myoblasts treated with 50  $\mu$ M UA, 10  $\mu$ M FCCP or vehicle (0.1% DMSO) ( $n = 4$ ). **(b)** Representative images ( $n = 5$ –10 images per group) and quantification of Mitosox fluorescence by FACS in C2C12 myoblasts treated with 50  $\mu$ M UA, 10  $\mu$ M rotenone (Rot-) or vehicle ( $n = 4$ ). For **a,b**, scale bars represent 20  $\mu$ m; **(c)** western blot of PINK1 and HSP90 in C2C12 myoblasts treated with 50  $\mu$ M UA, FCCP (10  $\mu$ M for 4 h) or vehicle ( $n = 3$  biological replicates). **(d)** Oxygen consumption at basal level and after injection of 1.25  $\mu$ M FCCP in C2C12 myotubes treated for 24 h with 20  $\mu$ M UA or vehicle in glycolytic medium (25 mM glucose) ( $n = 4$ ). **(e,f)** ATP content (**e**,  $n = 10$ ) and citrate synthase activity (**f**,  $n = 9$ ) in C2C12 myoblasts treated with 50  $\mu$ M UA or vehicle. **(g)** Oxygen consumption in C2C12 myotubes treated for 24 h with 20  $\mu$ M UA or vehicle in glycolytic medium (25 mM glucose). Complex activity was stimulated/inhibited after the successive addition of: 1) pyruvate/malate/glutamate/NAD<sup>+</sup>; 2) succinate; 3) rotenone; 4) antimycin A. CI + II or CIII, respiratory CI and CII or CIII ( $n = 4$ ). \* $P \leq 0.05$ ; \*\*\* $P \leq 0.001$  for comparison versus vehicle by Student's *t*-test. **(h)** Oxygen consumption at basal level and after injection of 1.25  $\mu$ M FCCP in C2C12 myotubes treated for 24 h with 20  $\mu$ M UA or vehicle in fatty acid oxidation medium (2.5 mM glucose + 166  $\mu$ M palmitate) ( $n = 6$ ). **(i)** Western blot of C2C12 myoblasts treated with 50  $\mu$ M UA or vehicle ( $n = 3$  biological replicates). \* $P \leq 0.05$ , \*\* $P \leq 0.01$ , \*\*\* $P \leq 0.001$ ; for comparisons versus vehicle by Student's *t*-test (**d-h**) or one-way ANOVA (**a,b**). Values are mean  $\pm$  s.e.m. Data and images are representative of two (**c-i**) or three (**a,b**) independent experiments. See also **Supplementary Figure 6**.

Of note, compared with vehicle, we also found that UA extended lifespan in young or old worms exposed to paraquat (**Supplementary Fig. 5a–c**), an inducer of mitochondrial reactive oxygen species (ROS) production that was recently used to investigate the mitophagy pathway<sup>25</sup>. Together with our gene expression data (**Supplementary Fig. 4a**), this finding confirmed that UA activates mitophagy throughout the duration of the treatment. Furthermore, we found that UA had no effect on ROS production, as measured using the ROS-sensitive Mitosox dye (**Supplementary Fig. 5d**), and prolonged lifespan in the presence of the potent antioxidant *N*-acetylcysteine (**Supplementary Fig. 5e**), indicating that UA exerts its beneficial effects independent of ROS levels.

### UA induces mitophagy in mammalian cells

Extending these findings to mammals, we found that UA's ability to stimulate autophagy and mitophagy was conserved in mammalian cells derived from the two tissues in which UA showed an effect in worms: muscle and intestine. Specifically, we found that C2C12 myoblasts and Mode-K intestinal cells treated with UA showed a dose-dependent elevation of the biomarkers for autophagy (the ratio of LC3-II/LC3-I (ref. 29) in the total cell lysate) and mitophagy (ubiquitination and p62/SQSTM enrichment in the mitochondrial fraction) compared

to vehicle treatment ( $n = 3$  biological replicates; **Fig. 4a,b** and **Supplementary Fig. 6a,b**). UA exposure also resulted in higher levels of phospho-AMPK $\alpha$ , one of the kinases involved in autophagy initiation. In addition, a dose-dependent induction of autophagy by UA was observed in C2C12 myoblasts via fluorescence-activated cell sorting (FACS) analysis using an anti-LC3-II antibody (**Supplementary Fig. 6c**). The induction of autophagic flux following 24 h of UA treatment was confirmed using the lysosomal fusion inhibitor Bafilomycin A, which induced a marked accumulation of p62/SQSTM and LC3-II when combined with UA compared with UA alone ( $n = 3$  biological replicates; **Fig. 4c**). UA treatment also induced the formation of both endogenous autophagosomes<sup>30</sup>, as measured with the CytoID dye using FACS (**Fig. 4d** and **Supplementary Fig. 6d**), and autolysosomes, as observed by confocal microscopy in C2C12 myoblasts transfected with mRFP-GFP-LC3B construct<sup>31</sup> (**Fig. 4e**).

We further ascertained the presence of mitophagy using three complementary methods. First, we used confocal microscopy and found a colocalization of mitochondria and autophagosomes in UA- (50  $\mu$ M) or FCCP-treated (10  $\mu$ M during 2 h) cells (**Fig. 4f**), and a fragmentation of the mitochondrial network (**Fig. 4g**) after UA treatment. Second, we used FACS and the mitochondrial pHRed, a modified mKeima construct<sup>32,33</sup>, and found that UA treatment resulted in a

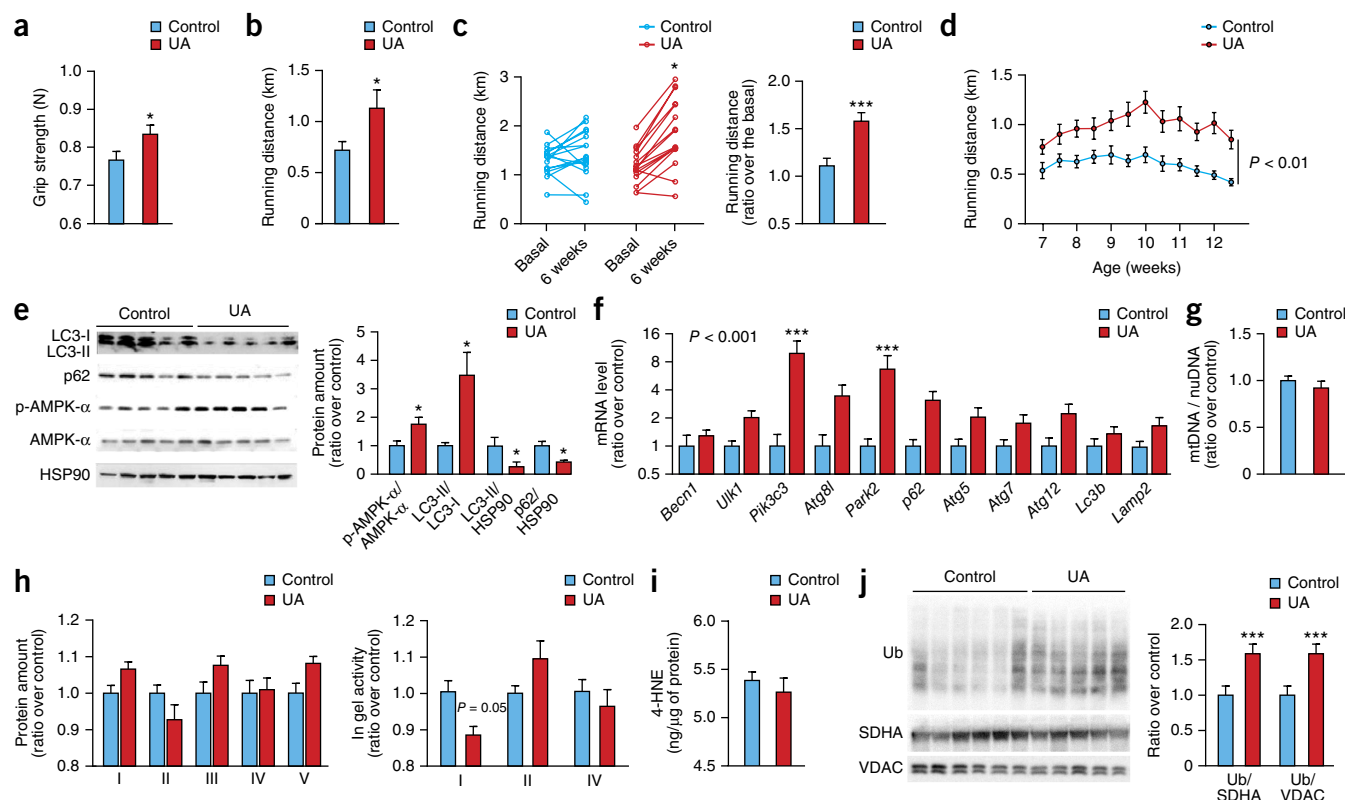


**Figure 6** UA improves exercise capacity in rodent models via the induction of mitophagy. (**a,b**) Grip strength (**a**,  $n = 25$ ) and overnight running distance in running wheels (**b**,  $n = 25$ ) in 23–24-month-old male C57BL/6J mice following UA treatment for 27 and 31 weeks, respectively, while on a HFD. (**c**) Exercise capacity on treadmill in 24-month-old male C57BL/6J mice treated with UA for 6 weeks while fed a NCD expressed as running distance (left;  $n = 16$ ) or as ratio over basal running distance (right;  $n = 16$ ). (**d**) Overnight running distance in running wheels in male Wistar Han rats during UA treatment on a NCD ( $n = 12$ ).  $P$  value is given for the comparison over the entire period of treatment after two-way ANOVA test. (**e–i**) Analysis in gastrocnemius muscles collected at the end of the experiment shown in **a,b**. (**e**) Western blot (left) and quantification of the bands in the gels (right) ( $n = 5$  biological replicates). (**f**) Quantification of autophagy and mitophagy genes expression ( $n = 10$ ).  $P$  value is given for the comparison over the entire panel of genes after two-way ANOVA test.  $***P \leq 0.001$  for comparison versus control after Bonferroni post-test. (**g**) Quantification of mtDNA/nuDNA ratio ( $n = 12$ ). (**h**) Quantification of respiratory complexes protein (I to V) (left) and activity (I, II and IV) (right) by BN-PAGE ( $n = 12$ ). (**i**) Quantification of 4-HNE, a by-product of lipid peroxidation and ROS ( $n = 12$ ). (**j**) Western blot of the gastrocnemius of male Wistar Han rats treated for 6 months on a NCD ( $n = 6$  biological replicates). Values are mean  $\pm$  s.e.m.  $*P \leq 0.05$ ,  $**P \leq 0.01$ ,  $***P \leq 0.001$ ; by Student's  $t$ -test (**a–c,e,j**). Control means the corresponding diet without UA admixed. See also **Supplementary Figure 7**.

significantly greater percentage of mitochondria inside the autolysosome measured compared with vehicle treatment (**Fig. 4h**). Finally, we found that mitochondrial content was lower by  $\sim 20\%$  following 24 h of UA compared with vehicle exposure, as quantified using the mtDNA/nDNA ratio (**Fig. 4i**).

One of the initial signals triggering mitophagy is the loss of mitochondrial membrane potential ( $\Delta\psi_M$ ), which leads to the stabilization of PINK-1 (ref. 34). We found that short-term treatment (1 and 4 h) of C2C12 myoblasts with UA lowered  $\Delta\psi_M$ , as measured by tetramethylrhodamine methyl ester (TMRE) fluorescence, compared with vehicle treatment (**Fig. 5a**), an effect that was independent of ROS production, as measured using the ROS-sensitive fluorescent probe MitoSox (**Fig. 5b**). Consistent with a loss of  $\Delta\psi_M$ , PINK-1 expression was induced in UA-treated C2C12 myoblasts ( $n = 3$  biological replicates; **Fig. 5c**). Notably, the effect of UA on  $\Delta\psi_M$  was not a result of an inhibition of the mitochondrial respiratory chain or uncoupling (**Supplementary Fig. 6e,f**). Long-term treatment (24 h) of C2C12 myotubes with UA, compared with vehicle, resulted in lower basal respiration while maximal respiratory capacity was maintained (**Fig. 5d**), as we observed in *C. elegans*. Consistent with this, ATP content and citrate synthase activity

were also lower in the UA-treated group versus the vehicle-treated one (**Fig. 5e,f**).

To understand how UA results in lower basal respiration following long-term treatment, the activity of the mitochondrial respiratory complexes was tested in intact cells by using specific substrates and inhibitors (**Fig. 5g**). Compared with vehicle, we found that long-term treatment (24 h) with UA resulted in lower respiration in the presence of pyruvate, malate, glutamate and nicotinamide adenine dinucleotide ( $\text{NAD}^+$ ) in C2C12 myotubes, indicating that it downregulates aerobic glycolysis and thereby indirectly inhibits complex I (CI) respiration (**Fig. 5g**). To test whether cells can compensate for this effect by shifting to complex II (CII)-driven respiration, we incubated C2C12 myotubes in a medium that stimulates fatty acid oxidation (glucose 2.5 mM + palmitate 166  $\mu$ M), and thereby the production of reduced flavin adenine dinucleotide ( $\text{FADH}_2$ ), a co-factor of CII (**Fig. 5h**). In this scenario, UA exposure resulted in greater cellular respiration under both basal and uncoupled conditions compared with vehicle treatment (**Fig. 5h**). Consistent with this observation, UA treated cells showed an approximately tenfold higher level of the CII subunit SDHB along with a four- to fivefold higher expression of subunits from complexes III, IV and V ( $n = 3$  biological replicates; **Fig. 5i** and



**Supplementary Fig. 6g**). Altogether, despite the decrease in aerobic glycolysis, there was an increase in mitochondrial chain subunits and CII-driven respiration, which explains how cells respond to the energetic demand in the wake of a lower mitochondrial content.

### UA induces mitophagy and improves muscle function in rodents

UA has been shown to pass the gastro-intestinal tract and enter plasma in rodents, and has been found in tissues such as liver, kidney and colon<sup>10,35</sup>. However, its bioavailability in skeletal muscle tissue has not been reported. Thus, we administered UA (25 mg per kg body weight per d (mg/kg/d)) to rats via their food and found detectable and stable UA levels in both plasma and vastus lateralis muscle after 2 and 7 d of treatment (**Supplementary Fig. 7a,b**). In light of the bioavailability of UA in the muscle, we evaluated UA treatment for the prevention of age-related muscle decline in 16-month-old male C57BL/6J mice fed a high-fat diet (HFD). From the age of 16 months onwards, we supplemented the diet with 50 mg/kg/d of UA for another 8 months. We found that chronic UA administration did not affect body weight gain or the evolution of fat and lean body mass (**Supplementary Fig. 7c**). UA treatment did not result in robustly greater muscle function measured at 22 and 24 months of age compared to the control HFD, in spite of the absence of changes in muscle mass, as manifested by a 9% greater grip strength and a 57% greater degree of spontaneous exercise measured using the running wheel ( $n = 25$  mice; **Fig. 6a,b**).

In a second mouse study, we assessed UA by treating aged male C57BL/6J mice (22.5 months old) that had been fed a normal chow diet (NCD) with a shorter 6-week treatment regimen. We performed a basal measurement of exercise capacity before treatment and randomized mice into UA and control groups fed with NCD. Mice were retested after 6 weeks of UA treatment at 24 months of age ( $n = 16$  mice; **Fig. 6c**). Notably, UA led to an average 42% greater running endurance ( $n = 16$  mice; **Fig. 6c**). In addition, in these mice fed with either control or UA-containing NCD, body weight or body composition was not affected (**Supplementary Fig. 7d,e**).

Following these observations in aging mouse models, we assessed the effect of UA on muscle function in young rats. Male Wistar rats were fed with NCD containing UA at a concentration of 25 mg/kg/d starting at 5.5 weeks of age. We assessed muscle function by measuring voluntary running in activity wheels to which the rats had access two nights per week from 7 weeks of age. Notably, rats were randomized for their activity level, as measured during an elevated plus maze test at the onset of the study (**Supplementary Fig. 7f**). On average, UA treatment resulted in a running capacity 65% greater than the control group ( $n = 12$  rats; **Fig. 6d**).

At the molecular level, we found that, compared with controls, UA stimulated autophagy in gastrocnemius muscle, as illustrated by a greater ratio of LC3-II to LC3-I and the concomitant lower p62/SQSTM levels (**Fig. 6e**), as well as a general tendency for an higher expression of autophagy (*Becn1*, *Ulk1*, *Pik3c3*, *Atg8l*, *p62*, *Atg5*, *Atg7*, *Atg12*, *Lc3b* and *LAMP2*) and mitophagy (*Park2*) transcripts (**Fig. 6f**). UA also induced the phosphorylation of AMPK in muscle tissue ( $n = 5$  biological replicates; **Fig. 6e**). In contrast, we found no significant differences in transcript levels of the myosin heavy chain types (**Supplementary Fig. 7g**), confirming that the improvement of muscle function is not a result of a change in muscle fiber type. UA did not change mtDNA/nuDNA ratio (**Fig. 6g**) or respiratory complexes abundance at the protein level (**Fig. 6h** and **Supplementary Fig. 7h**) in the gastrocnemius. However, evaluation of assembled OXPHOS complexes (by BN-PAGE) and activity (by in-gel activity assay) showed a lower amount of assembled CI and a tendency for greater CII activity

(**Fig. 6h** and **Supplementary Fig. 7i,j**) in the UA-treated versus control group, consistent with what was observed in cells. Finally, as in worms and cells, UA did not affect ROS levels in the muscle, as revealed by 4-hydroxynonenal (4-HNE) quantification (**Fig. 6i**).

As a result of insufficient quantities of muscle tissue available in mice, we were unable to test mitochondrial fractions for ubiquitination, a post-translational modification that is known to be associated with mitophagy<sup>36–38</sup>. Consequently, we assessed by western blot the mitochondrial fraction in muscles of male Wistar rats treated with chow diet containing UA compared with controls, and found a greater level of ubiquitinated mitochondrial proteins in the gastrocnemius in the UA-treated group ( $n = 6$  biological replicates; **Fig. 6j**).

### DISCUSSION

Optimal mitochondrial activity is essential for the production of cellular energy and the metabolic flexibility of an organism. During aging, there is a progressive decline in mitochondrial function that correlates with the load of mtDNA mutations<sup>39</sup>. Another hallmark of aging is the gradual decay of protein homeostasis, or proteostasis, notably through the decrease in autophagy<sup>40</sup>. Mitophagy, a specific form of autophagy by which cells eliminate their damaged mitochondria<sup>34</sup>, is at the crossroad between these two key hallmarks of aging, making it a compelling therapeutic target for managing the specific health complications associated with aging. Present therapeutic approaches targeting improved mitochondrial function have been designed to stimulate either mitochondrial biogenesis or the respiratory chain, whereas no specific and safe inducer of mitophagy has been described to date<sup>41</sup>. We found that UA potently induced mitophagy in *C. elegans*, mammalian cells and rodents, resulting in an overall improvement of multiple cellular and organismal phenotypes (**Supplementary Fig. 8a**).

In young worms and mammalian cells, the short-term administration of UA decreased the mitochondrial content while maintaining the maximal respiratory capacity. This confirmed that, despite the reduction in the mitochondrial pool following UA treatment, the remaining mitochondria are robust and able to sustain energy needs, potentially by shifting respiration from CI to CII as seen in mammalian cells (**Supplementary Fig. 8b–d**). Notably, a similar shift in respiration from CI to CII during the induction of mitophagy has also been observed in the heart during the perinatal period in mice<sup>42</sup>. Following long-term exposure, worms responded to the UA-mediated mitophagy by inducing mitochondrial biogenesis. In fact, it has been shown that a coordinated regulation of mitophagy and mitochondrial biogenesis in worms occurs through the *skn-1* transcription factor<sup>25</sup>. This induction of mitophagy in worms by UA led to an improvement of respiratory capacity, mobility and pharyngeal pumping. Our data furthermore suggest that the induction of mitophagy early in life may lead to an increase in mitochondrial content later in life.

Long-term oral administration of UA to rodents also induced mitophagy in the muscle of both young and old animals. This resulted in an enhanced exercise capacity in young rats, whereas UA administration in a NCD or HFD in aged mice, by prevention and intervention modalities, both enhanced muscle strength and robustly augmented running endurance without increasing lean muscle mass. This supports the hypothesis that UA improves muscle cell quality rather than quantity. It also indicates that UA's effect on muscle function is independent of the diet composition. Furthermore, these rodent studies highlight that UA improves muscle function throughout the different stages of life after a relatively short-term intervention. Notably, the *in vivo* results were obtained after administration of UA at a dose of



50 mg/kg/d in mice, which is equivalent to 4 mg/kg/d in humans<sup>43</sup> and is within standard human dosing regimens employed for both nutrition and pharmaceutical active ingredients.

From a mechanistic angle, it is interesting to point out that UA induces mitophagy subsequently to a reduction in membrane potential. Notably, recent studies with mitochondrial uncouplers, such as niclosamide ethanolamine (NEN) and 2,4-dinitrophenol (DNP), demonstrated beneficial effects of uncoupling specifically on systemic metabolism<sup>44–46</sup>. Although those studies were mainly focused on the liver and did not evaluate the potential contributions of autophagy and mitophagy, there may be some similarities between both the subcellular effects and organismal benefits of UA and these mitochondrial uncouplers that merit further study.

In the clinic, decreased mitophagy in skeletal muscle has been linked to reduced mobility in the elderly. This decline in muscle function observed in the elderly is often part of a larger syndrome, termed frailty, which is an important risk factor for disability, hospitalization and mortality<sup>47</sup>. A decline in mitophagy in the muscle has been proposed to explain muscle weakness in the elderly, and, in fact, a decrease in mitophagy-related gene expression was reported to correlate with slower walking speed in frail elderly<sup>48</sup>.

Current therapeutic strategies to prevent or treat muscle weakness and loss have mainly focused on improving muscle mass either through dietary intervention via supplements consisting of blends of proteins and amino acids or by pharmaceutical approaches targeting the myostatin pathway<sup>49,50</sup>. An investigation by meta-analysis of the clinical effectiveness of protein and amino acid supplementation in the elderly revealed that this approach alone is insufficient to increase body lean mass and muscle strength<sup>51</sup>. Very recently, a promising antibody drug candidate targeting the myostatin pathway failed in late-stage clinical studies in the muscle-wasting disease sporadic inclusion body myositis<sup>52</sup>. These observations suggest that modulation of muscle mass alone may not be sufficient to provide a clinically relevant effect on mobility. Improvement of muscle quality by enhancing mitochondrial function, as seen here with UA, instead of or together with muscle quantity may be an alternative strategy for treating impaired muscle functionality. Our data advocate that nutritional supplementation with UA to induce mitophagy holds promise for further development in humans as an innovative approach for improving mitochondrial and muscle function.


## METHODS

Methods and any associated references are available in the [online version of the paper](#).

**Accession codes.** Protein Data Bank: Coordinates have been deposited with accession code XXXX. 

Note: Any Supplementary Information and Source Data files are available in the [online version of the paper](#).


## ACKNOWLEDGMENTS

 We thank P. Gönczy (Swiss Institute for Experimental Cancer Research, Ecole Polytechnique Fédérale de Lausanne) for sharing reagents and equipment, the *Caenorhabditis* Genetics Center for providing worm strains and the Auwerx team members for discussions. We thank K.H. Kim (Yonsei University College of Medicine) for providing mRFP-GFP-LC3B reporter and for discussion. We thank G. Yellen (Department of Neurobiology, Harvard Medical School) for providing mitochondrial pHRed expressing plasmid. J.A. is the Nestlé Chair in Energy Metabolism. Work in the Auwerx laboratory is supported by the Ecole Polytechnique Fédérale de Lausanne and Systems X (SysX.ch 2013/153), and was co-financed by the Commission for Technology and Innovation (CTI) (15171.1 PFLS-LS). L.M. was supported by a fellowship from Fondation Médicale pour la Recherche (FRM).

## AUTHOR CONTRIBUTIONS

L.M., P.A.A., D.R., P.A., C.S., C.R. and J.A. conceived and designed the project. L.M., P.A.A., D.R., E.K., A.A.N.-d.-F., P.J., G.L.S., N.M., E.G.W. and D.H. performed the experiments. L.M., C.R., P.A.A. and J.A. wrote the manuscript, with contributions from all of the other authors.

## COMPETING FINANCIAL INTERESTS

The authors declare competing financial interests: details are available in the [online version of the paper](#). 

Reprints and permissions information is available online at <http://www.nature.com/reprints/index.html>.

- Cordain, L. *et al.* Plant–animal subsistence ratios and macronutrient energy estimations in worldwide hunter-gatherer diets. *Am. J. Clin. Nutr.* **71**, 682–692 (2000).
- Bakkalbasi, E., Mentes, O. & Artik, N. Food ellagitannins—occurrence, effects of processing and storage. *Crit. Rev. Food Sci. Nutr.* **49**, 283–298 (2009).
- Johanningsmeier, S.D. & Harris, G.K. Pomegranate as a functional food and nutraceutical source. *Annu. Rev. Food Sci. Technol.* **2**, 181–201 (2011).
- Espín, J.C., Larrosa, M., García-Conesa, M.T. & Tomás-Barberán, F. Biological significance of urolithins, the gut microbial ellagic acid–derived metabolites: the evidence so far. *Evid. Based Complement. Alternat. Med.* **2013**, 270418 (2013).
- Seeram, N.P. *et al.* Pomegranate juice ellagitannin metabolites are present in human plasma and some persist in urine for up to 48 hours. *J. Nutr.* **136**, 2481–2485 (2006).
- Núñez-Sánchez, M.A. *et al.* Targeted metabolic profiling of pomegranate polyphenols and urolithins in plasma, urine and colon tissues from colorectal cancer patients. *Mol. Nutr. Food Res.* **58**, 1199–1211 (2014).
- Truchado, P. *et al.* Strawberry processing does not affect the production and urinary excretion of urolithins, ellagic acid metabolites, in humans. *J. Agric. Food Chem.* **60**, 5749–5754 (2012).
- González-Sarriá, A. *et al.* Occurrence of urolithins, gut microbiota ellagic acid metabolites and proliferation markers expression response in the human prostate gland upon consumption of walnuts and pomegranate juice. *Mol. Nutr. Food Res.* **54**, 311–322 (2010).
- Tomás-Barberán, F.A., García-Villalba, R., González-Sarriá, A., Selma, M.V. & Espín, J.C. Ellagic acid metabolism by human gut microbiota: consistent observation of three urolithin phenotypes in intervention trials, independent of food source, age and health status. *J. Agric. Food Chem.* **62**, 6535–6538 (2014).
- Seeram, N.P. *et al.* Pomegranate ellagitannin-derived metabolites inhibit prostate cancer growth and localize to the mouse prostate gland. *J. Agric. Food Chem.* **55**, 7732–7737 (2007).
- Piowowski, J.P., Kiss, A.K., Granica, S. & Moeslinger, T. Urolithins, gut microbiota-derived metabolites of ellagitannins, inhibit LPS-induced inflammation in RAW 264.7 murine macrophages. *Mol. Nutr. Food Res.* **59**, 2168–2177 (2015).
- Kang, I., Kim, Y., Tomás-Barberán, F.A., Espín, J.C. & Chung, S. Urolithin A, C and D, but not iso-urolithin A and urolithin B, attenuate triglyceride accumulation in human cultures of adipocytes and hepatocytes. *Mol. Nutr. Food Res.* **60**, 1129–1138 (2016).
- Kenyon, C.J. The genetics of aging. *Nature* **464**, 504–512 (2010).
- Cabreiro, F. *et al.* Metformin retards aging in *C. elegans* by altering microbial folate and methionine metabolism. *Cell* **153**, 228–239 (2013).
- Wilkinson, D.S., Taylor, R.C. & Dillin, A. Analysis of aging in *Caenorhabditis elegans*. *Methods Cell Biol.* **107**, 353–381 (2012).
- Kenyon, C., Chang, J., Gensch, E., Rudner, A. & Tabtiang, R. A *C. elegans* mutant that lives twice as long as wild type. *Nature* **366**, 461–464 (1993).
- Lakowski, B. & Hekimi, S. The genetics of caloric restriction in *Caenorhabditis elegans*. *Proc. Natl. Acad. Sci. USA* **95**, 13091–13096 (1998).
- Dillin, A. *et al.* Rates of behavior and aging specified by mitochondrial function during development. *Science* **298**, 2398–2401 (2002).
- Lin, K., Dorman, J.B., Rodan, A. & Kenyon, C. daf-16: an HNF-3/forkhead family member that can function to double the life-span of *Caenorhabditis elegans*. *Science* **278**, 1319–1322 (1997).
- Apfeld, J., O'Connor, G., McDonagh, T., DiStefano, P.S. & Curtis, R. The AMP-activated protein kinase AAK-2 links energy levels and insulin-like signals to lifespan in *C. elegans*. *Genes Dev.* **18**, 3004–3009 (2004).
- Ishii, N. *et al.* A mutation in succinate dehydrogenase cytochrome b causes oxidative stress and aging in nematodes. *Nature* **394**, 694–697 (1998).
- Kang, C., You, Y.J. & Avery, L. Dual roles of autophagy in the survival of *Caenorhabditis elegans* during starvation. *Genes Dev.* **21**, 2161–2171 (2007).
- Hansen, M. *et al.* A role for autophagy in the extension of lifespan by dietary restriction in *C. elegans*. *PLoS Genet.* **4**, e24 (2008).
- Meléndez, A. *et al.* Autophagy genes are essential for dauer development and life-span extension in *C. elegans*. *Science* **301**, 1387–1391 (2003).
- Palikaras, K., Lionaki, E. & Tavernarakis, N. Coordination of mitophagy and mitochondrial biogenesis during aging in *C. elegans*. *Nature* **521**, 525–528 (2015).
- Chan, D.C. Fusion and fission: interlinked processes critical for mitochondrial health. *Annu. Rev. Genet.* **46**, 265–287 (2012).
- Lackner, L.L. & Nunnari, J. Small-molecule inhibitors of mitochondrial division: tools that translate basic biological research into medicine. *Chem. Biol.* **17**, 578–583 (2010).

28. Kirienko, N.V., Ausubel, F.M. & Ruvkun, G. Mitophagy confers resistance to siderophore-mediated killing by *Pseudomonas aeruginosa*. *Proc. Natl. Acad. Sci. USA* **112**, 1821–1826 (2015).
29. Yang, Z. & Klionsky, D.J. Eaten alive: a history of macroautophagy. *Nat. Cell Biol.* **12**, 814–822 (2010).
30. Guo, S. *et al.* A rapid and high content assay that measures cyto-ID-stained autophagic compartments and estimates autophagy flux with potential clinical applications. *Autophagy* **11**, 560–572 (2015).
31. Mizushima, N., Yoshimori, T. & Levine, B. Methods in mammalian autophagy research. *Cell* **140**, 313–326 (2010).
32. Lazarou, M. *et al.* The ubiquitin kinase PINK1 recruits autophagy receptors to induce mitophagy. *Nature* **524**, 309–314 (2015).
33. Tantama, M., Hung, Y.P. & Yellen, G. Imaging intracellular pH in live cells with a genetically encoded red fluorescent protein sensor. *J. Am. Chem. Soc.* **133**, 10034–10037 (2011).
34. Youle, R.J. & Narendra, D.P. Mechanisms of mitophagy. *Nat. Rev. Mol. Cell Biol.* **12**, 9–14 (2011).
35. Gasperotti, M. *et al.* Fate of microbial metabolites of dietary polyphenols in rats: is the brain their target destination? *ACS Chem. Neurosci.* **6**, 1341–1352 (2015).
36. Kirkin, V., McEwan, D.G., Novak, I. & Dikic, I. A role for ubiquitin in selective autophagy. *Mol. Cell* **34**, 259–269 (2009).
37. Lee, J.Y., Nagano, Y., Taylor, J.P., Lim, K.L. & Yao, T.P. Disease-causing mutations in parkin impair mitochondrial ubiquitination, aggregation and HDAC6-dependent mitophagy. *J. Cell Biol.* **189**, 671–679 (2010).
38. Bingol, B. *et al.* The mitochondrial deubiquitinase USP30 opposes parkin-mediated mitophagy. *Nature* **510**, 370–375 (2014).
39. Bratic, A. & Larsson, N.G. The role of mitochondria in aging. *J. Clin. Invest.* **123**, 951–957 (2013).
40. Rubinsztein, D.C., Mariño, G. & Kroemer, G. Autophagy and aging. *Cell* **146**, 682–695 (2011).
41. Andreux, P.A., Houtkooper, R.H. & Auwerx, J. Pharmacological approaches to restore mitochondrial function. *Nat. Rev. Drug Discov.* **12**, 465–483 (2013).
42. Gong, G. *et al.* Parkin-mediated mitophagy directs perinatal cardiac metabolic maturation in mice. *Science* **350**, aad2459 (2015).
43. Center for Drug Evaluation and Research. Guidance for industry: estimating the maximum safe starting dose in initial clinical trials for therapeutics in adult healthy volunteers. *Food and Drug Administration* <http://www.fda.gov/downloads/Drugs/...Guidances/UCM078932.pdf> (2005).
44. Perry, R.J., Zhang, D., Zhang, X.M., Boyer, J.L. & Shulman, G.I. Controlled-release mitochondrial protonophore reverses diabetes and steatohepatitis in rats. *Science* **347**, 1253–1256 (2015).
45. Tao, H., Zhang, Y., Zeng, X., Shulman, G.I. & Jin, S. Niclosamide ethanolamine-induced mild mitochondrial uncoupling improves diabetic symptoms in mice. *Nat. Med.* **20**, 1263–1269 (2014).
46. Perry, R.J. *et al.* Reversal of hypertriglyceridemia, fatty liver disease and insulin resistance by a liver-targeted mitochondrial uncoupler. *Cell Metab.* **18**, 740–748 (2013).
47. Fried, L.P. *et al.* Frailty in older adults: evidence for a phenotype. *J. Gerontol. A Biol. Sci. Med. Sci.* **56**, M146–M156 (2001).
48. Drummond, M.J. *et al.* Downregulation of E3 ubiquitin ligases and mitophagy-related genes in skeletal muscle of physically inactive, frail older women: a cross-sectional comparison. *J. Gerontol. A Biol. Sci. Med. Sci.* **69**, 1040–1048 (2014).
49. Robinson, S., Cooper, C. & Aihie Sayer, A. Nutrition and sarcopenia: a review of the evidence and implications for preventive strategies. *J. Aging Res.* **2012**, 510801 (2012).
50. Amato, A.A. *et al.* Treatment of sporadic inclusion body myositis with bimagrumab. *Neurology* **83**, 2239–2246 (2014).
51. Xu, Z.R., Tan, Z.J., Zhang, Q., Gui, Q.F. & Yang, Y.M. Clinical effectiveness of protein and amino acid supplementation on building muscle mass in elderly people: a meta-analysis. *PLoS One* **9**, e109141 (2014).
52. Garber, K. No longer going to waste. *Nat. Biotechnol.* **34**, 458–461 (2016).
53. Kim, S.J. *et al.* CRIF1 is essential for the synthesis and insertion of oxidative phosphorylation polypeptides in the mammalian mitochondrial membrane. *Cell Metab.* **16**, 274–283 (2012).
54. Greber, B.J. *et al.* Architecture of the large subunit of the mammalian mitochondrial ribosome. *Nature* **505**, 515–519 (2014).

#### COMPETING FINANCIAL INTERESTS

P.A.A. and C.R. are employed by Amazenit; C.R. and P.A. are board members of Amazenit; and J.A. and C.S. are consultants to Amazenit.

#### EDITORIAL SUMMARY

**AOP:** The naturally occurring compound urolithin A has been found to promote mitophagy, thereby increasing lifespan in worms and improving skeletal muscle activity in rodents.

## ONLINE METHODS

***C. elegans* strains and RNAi experiments.** *C. elegans* strains were cultured at 20 °C on nematode growth media agar plates seeded with *E. coli* strain OP50 unless stated otherwise. Strains used in this study are listed in the **Supplementary Table 3**. Strains were provided by the Caenorhabditis Genetics Center (University of Minnesota). Bacterial feeding RNAi experiments were carried out as described<sup>55</sup>. Clones used were *bec-1* (T19E7.3), *dct-1* (C14F5.1), *pink-1* (EEED8.9), *skn-1* (T19E7.2), *sqst-1* (T12G3.1) and *vps-34* (B0025.1). Clones were purchased from GeneService and sequenced.

**Pharmacological treatment of *C. elegans*.** EA and urolithin metabolites were provided by Amazentis SA. Compounds: EA (2,3,7,8-tetrahydroxy-chromeno[5,4,3-cde]chromene-5,10-dione; EA), urolithin A (3,8-dihydroxy-6H-dibenzo[b,d]pyran-6-one; UA), urolithin B (3-hydroxy-6H-dibenzo[b,d]pyran-6-one; UB), urolithin C (3,7,8-trihydroxy-6H-dibenzo[b,d]pyran-6-one; UC) and urolithin D (3,4,8,9-tetrahydroxy-6H-dibenzo[b,d]pyran-6-one; UD) were added at the indicated concentration just before pouring the plates. Worms were exposed to compounds during the full life from eggs until death, unless stated otherwise. To ensure a permanent exposure to the compound, plates were changed twice a week. All the compounds used in this study were dissolved in a DMSO stock solution. The control population was treated with the corresponding concentration of DMSO at 1% final.

**Worm survival assays. Lifespan.** Lifespan tests were performed at 20 °C as described<sup>56</sup>. Worms that crawled off the plate or had an exploded vulva phenotype were censored. These exclusion criteria were established before starting the experiments.

The UV treatment of bacteria was performed as previously described with slight modifications<sup>14</sup>. Briefly, 80 µl of 5× concentrated *E. coli* OP50 suspension was seeded onto an NGM plate and then irradiated for 5 min on a UV Stratalinker 2400 (Stratagene) containing bulbs irradiating at 254 nm. Plates were further irradiated for 5 min on the day of transfer. The worm population was transferred every 2 d during the lifespan assay.

**Paraquat resistance.** 1-d-old or 8-d-old adult worms treated with UA were transferred on NGM plates seeded with *E. coli* OP50 containing paraquat at the final concentration of 4 mM. Animals were scored for survival every day.

**Worm phenotypic assays. Mobility.** *C. elegans* movement was performed as described<sup>57</sup> at days 1, 3, 5 and 8 of adulthood, using a modified version of the Parallel Worm Tracker for MATLAB<sup>57</sup>. The experiment was repeated at least twice.

**Pharyngeal pumping.** 50 synchronized adult worms per condition were transferred on NGM agar plates (10 worms per plate). After 1, 7 or 14 d of adulthood, the pharyngeal pumping was measured by counting the contraction of the pharynx during a period of 30 s, repeated twice. For each measurement, 8–10 worms were randomly analyzed among the worm population. The experiment was done twice on 8–10 individual worms randomly selected among the five plates.

**Development.** 50 adult worms per condition were transferred on NGM agar plates (10 worms per plate) and allowed to lay eggs for 3 h. Then they were removed and the number of eggs per plate was counted. 48 and 72 h later, the number of L1–L3 larvae, L4, young adults and adult worms was counted. The experiment was done twice with five individual plates containing ten worms each.

**Fertility.** Five L4 worms per condition were laid on NGM agar plates (1 L4 per plate) and allowed to lay eggs for 24 h. The eggs were counted and each mother was transferred on a new plate. These steps were repeated for 5 d. The experiment was done twice with five individual plates containing one worm each.

**Bacterial growth and avoidance assays.** Liquid bacterial growth was performed in 96-well plates containing the respective bacterial strain (previously grown overnight in LB and diluted 1,000-fold) and compounds in 200 µl of LB. Absorbance (OD 595 nm) was measured every hour over an 8-h period with shaking at 37 °C using a Victor X4 plate reader (Perkin Elmer). A total of five replicates were used per condition. Each experiment was repeated twice.

To assess the avoidance for compounds, DMSO and UA at 50 µM were mixed with a bacterial solution of OP50 and each solution was seeded on two sides of the plate. Then, a drop of M9 containing 50 worms was added in the mid-

dle of the plates. Every 2 h, the number of worms at each spot was counted. The experiment was repeated twice on three independent plates containing 50 worms each.

**Quantification of GFP signal in *C. elegans*.** GFP expression and quantification were carried out as described<sup>57</sup>. At least four wells containing 20 worms were quantified in each experiment. Each experiment was repeated at least twice.

**Mitoxox staining in *C. elegans*.** Mitoxox staining was performed as described<sup>57</sup>. Briefly, a population of 100 worms was recovered in 1 ml of M9 buffer, washed three times to remove residual bacteria, and resuspended in 200 µl of 1:200 Mitoxox stock solution (initial stock solution was dissolved at 1 mM in DMSO). After 20 min of treatment, worms were washed five times in 1 ml of M9 buffer to eliminate the Mitoxox reagent, and then transferred in a black-walled 96-well plate for reading.

**Confocal microscopy and image processing.** Cells were fixed with Formal-Fixx (Thermo Scientific) and permeabilized with 0.4% Triton for 5 min. Images of worms and cells were acquired using Zeiss LSM 700 Upright confocal microscope (Carl Zeiss AG) under non-saturating exposure conditions. Worms were prepared for imaging as described<sup>58</sup>. All snapshots were taken from the same part of *C. elegans*: intestinal cells from the upper part of the worm, excluding the regions of the vulva. For each condition up to 20 worms were observed and imaged. Tracing of the mitochondrial network contour was done by the use of Gaussian blur filter followed by the application of Laplacian operator. Image processing was performed with the Fiji software (<http://imagej.nih.gov/ij/>; version 1.47b). Each experiment was repeated at least twice.

**Oxygen-consumption assays. *C. elegans*.** Oxygen consumption was measured using the Seahorse XF96 equipment (Seahorse Bioscience) as described<sup>57</sup>. Respiration rates were normalized to the number of worms in each individual well. Each experiment was repeated at least twice.

**Cells.** Oxygen consumption was measured using the Oxygraph-2k (Oroboros Instruments) or the XF96 Extracellular Flux Analyzer. Differentiated C2C12 cells were trypsinized, counted and resuspended in complete DMEM medium. For the respiration through different respiratory complexes, differentiated C2C12 cells were resuspended in complete DMEM medium. The rates of respiration were measured after successive addition of 5 mM pyruvate, 2 mM malate, 10 mM glutamate and 2.5 mM ADP (respiration through complex I); 10 mM succinate (respiration through complex I and II); 0.5 µM rotenone (respiration through complex II); and 2.5 µM antimycin A for residual oxygen consumption. In a separate experiment, FCCP was injected at the final concentration of 1.25 µM after the addition of 5 mM pyruvate, 2 mM malate, 10 mM glutamate and 2.5 mM ADP and 10 mM succinate (respiration through complex I and II) to assess the maximal respiratory capacity (RC). All the measurements were done during 10 min at 37 °C in four different respiration chambers per condition. Values were normalized by the total number of cells in the chamber. This experiment was repeated three times.

For measurement of the acute effect of UA on respiration, oxygen consumption was measured using the XF96 Extracellular Flux Analyzer. Fully differentiated C2C12 myotubes were injected with increasing concentrations of UA at the beginning of the assay. Oxygen consumption was followed for 2 h. The assay was repeated in two independent experiments.

CII-driven respiration was assessed in C2C12 myotubes using the XF96 Extracellular Flux Analyzer. Once fully differentiated in a 96-well plate, C2C12 myotubes were treated in DMEM-based substrate limited medium, containing 0.5 mM glucose, 1 mM GlutaMAX, 0.5 mM carnitine, for 24 h. 45 min before the assay, cells were washed two times with Assay Medium (111 mM NaCl, 4.7 mM KCl, 1.25 mM CaCl<sub>2</sub>, 2 mM MgSO<sub>4</sub>, 1.2 mM NaH<sub>2</sub>PO<sub>4</sub>, 2.5 mM glucose, 0.5 mM carnitine, and 5 mM HEPES, adjusted to pH 7.4 at 37 °C on the day of the assay). Cells were then incubated for 30 min in a non-CO<sub>2</sub> incubator. Just before starting the assay, cells were supplemented with XF Palmitate-BSA FAO Substrate (Seahorse Bioscience) at a final concentration of 166 µM palmitate. Oxygen consumption rate was determined at basal level, and after the addition of FCCP at 10 µM. The assay was repeated in two independent experiments.

**Isolated mitochondria.** Mitochondria were isolated from mouse liver as described<sup>59</sup>. Oxygen consumption was measured using 4 µg of mitochondrial



proteins in the XF24 Extracellular Flux Analyzer. Mitochondria were resuspended in 500  $\mu$ l of MAS buffer (sucrose 70 mM, mannitol 220 mM,  $\text{KH}_2\text{PO}_4$  5 mM,  $\text{MgCl}_2$  5 mM, Hepes 2 mM, EGTA 1 mM, fatty-acid free BSA 0.2%) and added in succinate 2 mM and pyruvate 10 mM before measuring oxygen consumption rate. The assay was repeated in two independent experiments.

**Quantification of ATP levels and citrate synthase enzymatic activity.** Total ATP content and citrate synthase (CS) enzymatic activity were measured as described<sup>57</sup>. Briefly, total ATP content was measured by the CellTiter-Glo luminescent cell viability assay (Promega), and CS was determined using the CS assay kit (Sigma). Each experiment was repeated twice.

**Extraction of mRNA and DNA for quantitative real-time PCR.** *C. elegans*. A total of  $\approx$ 500 worms per conditions were manually recovered from 15 NGM plates and split into three biological replicates. Each experiment was repeated twice. Total RNA was prepared using TRIzol (Invitrogen) according to the manufacturer's instructions.

**Cells.** C2C12 myoblasts were grown in 6-well plates, with three biological replicates per condition per experiment. Each experiment was repeated twice. Total RNA was prepared using TRIzol (Invitrogen). DNA was extracted using the NucleoSpin kit (M&N) according to the instructions.

**Mouse muscle.** Total RNA was prepared using TRIzol (Invitrogen). For DNA extraction, approximately 15mg of muscle was incubated overnight at 55 °C in 500  $\mu$ l of DNA lysis buffer (100 mM NaCl, 20 mM Tris pH7.4, 10 mM, EDTA, 0.5% SDS) supplemented with Proteinase K at 400  $\mu$ g/ml. RNA was removed by treating the samples with RNase A (8.5 UI/mg) at 45  $\mu$ g/ml for 30 min at 37 °C. Samples were centrifuged for 5 min at 12,000g to recover the supernatant. DNA was precipitated by adding 250  $\mu$ l of ammonium acetate 7.5 M and 600  $\mu$ l of isopropanol, and pelleted by centrifuging at 12,000g for 10 min at 4 °C. The DNA pellet was washed with Ethanol 70% and centrifuged again at 12,000 g for 5 min at 4 °C.

**Quantitative real-time PCR for gene expression and mtDNA/nuDNA ratio.** cDNA was prepared using the QuantiTect Reverse Transcription Kit (Qiagen) following the manufacturer's instructions. The RT-qPCR reactions were performed using the Light-Cycler system (Roche Applied Science) and a qPCR Supermix (Qiagen) with the indicated primers (Supplementary Tables 4 and 5).

*C. elegans. act-1* and Y45F10D.4 were used as normalization controls for gene expression. Absolute quantification of the mtDNA copy number in worms was performed by real-time PCR as previously described<sup>60</sup>. Relative values for *nd-1* and *act-3* were compared within each sample to generate a ratio representing the relative level of mtDNA per nuclear genome. The results obtained were confirmed with a second mitochondrial gene MTCE.26. The average of at least three technical repeats was used for each biological data point. Each experiment was performed at least on four independent biological samples.

**Cells and mouse muscle.** mRNA levels were normalized over *B2m*, *Rplp1* and *Actb* for gene expression. Relative values for mitochondrial genes (*mt-Rnr2* and *mt-Co2*) and nuclear genes (*Ucp2* and *Hk2*) were compared in each sample to generate a ratio representing the relative level of mtDNA per nuclear genome (Supplementary Table 4). The average of two technical replicates was used for each biological data point.

**Isolation of mitochondria and blue native-PAGE using *C. elegans*.** One hundred mg worms were collected in M9 buffer, and were centrifuged at 600g for 5 min at 4 °C to remove the buffer. After discarding the buffer, worm pellets were washed three times with 1 $\times$  cold PBS. To homogenize, 2 ml of mitochondria isolation buffer (MIB, 10 mM Tris-HEPES, pH 7.4, 1 mM EGTA/Tris, pH 7.4, 200 mM Sucrose and Roche Complete Protease Inhibitor Cocktail Tablets) were added. Homogenization of the worms was performed using a Teflon Pestle (2 ml, Wheaton) at 1500 r.p.m (POLYMIX PX-SR 50 E stirrer, Kinematica) on ice. After 60 strokes, the worm-lysates were monitored under a microscope and unbroken worms and debris was removed by centrifugation at 600g for 10 min at 4 °C. The collected supernatants were centrifuged at 7,000g for 10 min at 4 °C to obtain mitochondrial fraction. After removing all supernatants, the pellets were washed once with 1 ml of MIB, and centrifuged at 7,000g for 10 min at 4 °C. The pellets were re-suspended with 100  $\mu$ l of MIB buffer for the

protein assay. 50  $\mu$ g of mitochondrial fraction was prepared by a centrifugation at 7,000g for 10 min at 4 °C, and re-suspended with 20  $\mu$ l of NativePAGE sample buffer with 0.5% n-dodecyl- $\beta$ -D-maltoside or 1% digitonin (Invitrogen). BN-PAGE was performed as previously described<sup>53</sup>. To detect OXPHOS complex, antibodies were selected based on the amino acid sequence-identity of the used immunogens to generate the antibodies. Anti-NDUFS3 antibody (1:1,000, ab14711, Abcam), anti-SDHA antibody (1:1,000, ab14715, Abcam), anti-SDHB antibody (1:1,000, ab14714, Abcam), anti-UQCRC2 (1:1,000, ab14745, Abcam), anti-MTCO1 (1:1,000, ab14705, Abcam) and anti-ATP5A (1:1,000, ab14748, Abcam) were used. After incubation in the primary antibody dilution, the membrane was washed and developed using the WesternBreeze Chromogenic Western Blot Immunodetection Kit (Invitrogen). This experiment was repeated at least twice.

**Quantification of mitochondrial respiratory complexes proteins and activity by BN-PAGE in mouse muscle.** BN-PAGE and In-Gel Activity was performed as described<sup>61</sup> with minor modifications. In brief, mitochondrial extracts were prepared as described<sup>59</sup>. For BN-PAGE, 25  $\mu$ g of mitochondria from gastrocnemius muscle was solubilized in n-dodecyl  $\beta$ -D-maltoside (DDM) and sample buffer (Invitrogen, BN 2008). DDM/protein ratio of 1.6 g/g was used. Electrophoresis was performed using Native PAGE Novex Bis-Tris Gel System (3–12%) for 3 h (30 min at 150 V and 2.5 h at 250 V). Gel transfer was performed using Invitrogen iBlot gel transfer system. For detection of the complexes, anti-oxphos cocktail (Invitrogen, 457999) and WesternBreeze Chromogenic Western Blot Immunodetection Kit (Invitrogen, WB7103) was used. For in-gel activity assays: CIV + CI activity was performed by subsequently incubating the gels in the substrate for CIV followed by incubation in CI. CII activity was performed on a separate gel. All reactions were stopped with 10% acetic acid. In-gel activity gels were used for quantification of individual complexes.

**Cell culture.** The well-established C2C12 cell line was chosen for the evaluation of the effect of UA on a muscle derived cell line and obtained from ATCC (CRL-1772). C2C12 myoblasts were cultured in Dulbecco's modified Eagle's medium (DMEM) including glucose 25 mM, 20% FCS and 50  $\mu$ g/ml gentamicin. Differentiation was induced for 4 d in Dulbecco's modified Eagle's medium (DMEM) including 25 mM glucose, 2% horse serum and 50  $\mu$ g/ml gentamicin. The Mode-K cell line derived from mouse intestinal epithelium was kindly supplied by Kaiserlian (INSERM)<sup>62</sup>. Cells were cultured in RPMI 1640 medium including glucose 25 mM, 10% FCS, 1 mM sodium pyruvate, 10 mM HEPES, 0.1 mM NEAA, 2-mercaptoethanol penicilline 100 UI/ml and streptomycin 100 g/ml. All cells were cultured at 37 °C under a 5%  $\text{CO}_2$  atmosphere and tested for mycoplasma using Mycoprobe (#CUL001B, R&D systems) following the manufacturer's instructions.

**Immunocytochemistry.** Immunocytochemistry was performed on Mode-K cells. Culture conditions are described above. Cells were transfected with GFP-LC3 (Addgene, #24920) construct for 24 h. The fixation was done with Formal-Fixx (Thermo Scientific), followed by permeabilization with 0.4% Triton. Cells were stained with rabbit polyclonal Tom20 (Santa Cruz Biotechnology, Sc-11415) primary antibody; and with rabbit Alexa 568 secondary antibody (Invitrogen). Autophagy flux was evaluated using mRFP-GFP-LC3B-expressing C2C12 myoblast. In one experiment, at least three different images (that is, two images including several cells and one image including a single cell) were taken per condition, with one well per condition. Images shown in figure are representative of the results obtained in four independent experiments.

**FACS analyses.** All FACS analyses were performed at least three times independently with BD LSR II Cell Analyzer. All analyses were done in ice-cold sorting buffer (1 $\times$  PBS including 25 mM HEPES, 10 mM glucose, 0.1% BSA) and each experiment includes approximately 50,000 events per group. The evaluations of endogenous autophagosome formation were done according to the manufacturer manual (CYTO-ID Autophagy detection kit, ENZ-51031, Enzo Life Sciences). Briefly, trypsinized cells were incubated with prepared Cyto-ID Green stain solution for 30 min at 37 °C in the dark with gentle agitation. After washing, stained cells were analyzed with a FITC filter (excitation 488 nm, emission 525 nm). Mitochondrial membrane potential and ROS generation evaluated with TMRM



and Mitosox Red, respectively. TMRM or Mitosox Red dye were added to cell-culture dishes, and incubated for 30 min at the cell culture incubator (5% CO<sub>2</sub>, 37 °C). Trypsinized cells were collected, washed and resuspended in ice-cold sorting buffer. Both TMRM and Mitosox Red stained cells were analyzed at 561-nm lasers with 586-nm emission filters. Geometric mean was calculated using fluorescence intensity values comprised between 10<sup>2</sup> and 10<sup>5</sup> A.U. The uncoupler FCCP was used as a positive control for TMRM staining. Rotenone, an inhibitor of complex I that triggers ROS, was used as a positive control for Mitosox staining. Mitophagy in live cells was monitored by evaluation of lysosomal (pH 4) mitochondrial pHRed (also known as mKeima-A213S) as described in the previous report<sup>32</sup>. Lysosomal mitochondrial pHRed in C2C12 myoblasts was quantified using dual-excitation ratiometric pH measurements at 488 nm (pH 7) and 561 nm (pH 4) lasers with 695/40 nm and 610/20 nm emission filters, respectively. Combination of 1 µg/ml oligomycin and 1.25 µM antimycin A was used as a positive control to trigger mitophagy. All FACS data were analyzed using software FlowJo and Flowing Software (<http://www.flowingsoftware.com/>).

**Determination of UA bioavailability in male Sprague-Dawley rats.** UA was admixed to AIN-93G Growing Rodent Diet (Research Diet, New Brunswick, NJ, USA) at a concentration of 0.25 g per kg of diet, corresponding to a dose of 25 mg/kg/d. Food pellets containing UA were given ad libitum for 7 d to male Sprague-Dawley rats, which were fitted with a jugular vein cannulation. A total of 18 rats (six rats per group) were housed in single cage. Blood was collected at time points 0, 2 and 7 d via the jugular vein cannula, placed into chilled tubes containing K<sub>3</sub>EDTA as the anticoagulant, and centrifuged at a temperature of 4 °C, at 3,000g, for 5 min to collect plasma. At time points 0, 2 and 7 d, separate cohorts of animals were killed and vastus lateralis was excised from both legs. Samples were analyzed by HPLC-MS/MS as described below. Procedures involving the care or use of animals in this study were conducted under the approved ASLP013-01 protocol by Absorption Systems LP (Exton) Institutional Animal Care and Use Committee.

**High-performance LC-electrospray ionization MS/MS analyses.** The concentration of UA was calculated using the internal standardization method. The area ratio of UA to the stable isotope-labeled internal standard [<sup>13</sup>C<sub>6</sub>]-UA against the concentration of calibration samples was used for quantification. The lower limit of quantification of this method was 0.1 ng/ml. The analysis was done by separation using reversed phase chromatography followed by detection with triple stage quadrupole MS/MS in the selected reaction monitoring mode. The HPLC-MS system consisted of the 1200 series HPLC pump (Agilent Technologies), equipped with an HTS PAL autosampler (CTC Analytics AG), a TSQ Vantage mass spectrometer, (Thermo Fisher Scientific) and a HotDog 5090 column oven (Prolab GmbH). Data were analyzed using LCQuan 2.5.6 and Xcalibur 2.0.7 (Thermo Fisher Scientific). The average of two technical replicates was used for each biological data point.

**Prevention and intervention on age-related decline in muscle function in aged C57BL/6J male mice.** For the prevention study, UA was admixed to D12492 (60 kcal% fat) HFD powder (Research Diet) at 0.5g per kg of diet, corresponding to a dose of 50 mg/kg/d. Pellets with or without UA were given to 16-month-old male C57BL/6J mice (Janvier) for 34 weeks. A total of 50 mice were housed by groups of 4 or 5 animals per cage and randomized to 25 animals per group according to their body weight and composition. Body composition was assessed by EchoMRI every 4 weeks starting from the beginning of the treatment. Grip strength was measured on forelimbs after 27 weeks of treatment using a Bioseb Grip Test device (Bioseb). Exercise capacity was assessed after 31 weeks of treatment by monitoring the overnight distance run in activity wheels with one mouse per cage. Mice were familiarized with running wheel for 24 h before recording the running activity. Animals were killed after 34 weeks of treatment after an overnight fasting before collecting gastrocnemius from both legs.

For the intervention study, UA was admixed to AIN-93G Growing Rodent Diet (Research Diet) at a concentration of 0.5 g per kg of diet, corresponding to a dose of 50 mg/kg/d. Pellets with or without UA were given to 22-month-old male C57BL/6J mice (Janvier) for 6 weeks. A total of 32 mice were housed individually and randomized to 16 animals per group according to their exercise

capacity. Body composition was assessed by EchoMRI every 3 weeks starting from the beginning of the treatment. Exercise capacity was assessed at basal level and after 6 weeks of treatment by measuring the endurance capacity of the animals, as previously described<sup>63</sup>. Experiments were authorized by the Veterinary office of the Canton of Vaud, Switzerland (authorization no. 2432). Animals that showed signs of severity predefined by the animal authorization no. 2432 were euthanized. These animals, together with those who died spontaneously during the experiments, were excluded from the calculations. These criteria were established before starting the experiments.

**Quantification of mitophagy in muscle and assessment of exercise capacity in male Wistar Han rats.** UA was admixed to AIN-93G Growing Rodent Diet (Research Diet) at a concentration of 0.25 g per kg of diet, corresponding to a dose of 25 mg/kg/d. Pellets with or without UA were given to 5.5-week-old male Wistar Han rats (Charles River, L'Arbresle, France). For the quantification of mitophagy in muscle, a total of 12 rats were randomized to six animals per group according to their body weight, housed by groups of two per cage and treated for 24 weeks. Animals were sacrificed after an overnight fasting before collecting gastrocnemius from both legs. The mitochondrial fraction was isolated from fresh tissue according to a protocol published previously<sup>59</sup> and analyzed by western blot. For the assessment of exercise capacity, a total of 24 rats were randomized to 12 animals per group according to their basal level of activity measured as velocity during an Elevated Plus Maze test at the age of 5.5 weeks, before starting the treatment. From the age of 7 weeks, rats were housed 2 nights per week in single cages equipped with an activity wheel connected to a sensor (Intellibio) for 6 weeks.

Experiments were authorized by the Veterinary office of the Canton of Vaud, Switzerland (authorization no. 2596). Animals that showed signs of severity predefined by the animal authorization no. 2596 were euthanized. These animals, together with those who died spontaneously during the experiments, were excluded from the calculations. These criteria were established before starting the experiments.

**4-HNE.** Approximately 10 mg of muscle was lysed using RIPA buffer (Cell Signaling) supplemented with protease inhibitors (Mini-Complete, Roche) and Tissue Lyser (Qiagen) at 30 shakes per s for 2 min. Cellular debris were pelleted at 12,000g for 10 min at 4 °C, and proteins were recovered in the supernatant. Proteins were quantified using DC Protein Assay (Bio-Rad). The concentration in 4-HNE was determined using OxiSelect™ HNE Adduct Competitive ELISA Kit (Cell Biolabs) following manufacturer's instructions. 12.5 µg of proteins per sample were loaded in duplicate.

**Western blot analysis.** Cells, mitochondrial proteins and tissue were lysed with RIPA buffer containing protease and phosphatase inhibitors, and analyzed by SDS-PAGE and western blot. Proteins were detected using the specific antibodies listed in **Supplementary Table 6**. In addition to the housekeeping proteins, loading was monitored by Ponceau Red to ensure a homogeneous loading. Pixel intensity was quantified by using ImageJ software.

**Statistical analyses.** Survival analyses were performed using the Kaplan Meier method and the significance of differences between survival curves calculated using the log rank test. When appropriate ( $n > 8$ ), Shapiro-Wilk normality test was used to assess normal distribution of the samples. Differences between two groups were assessed using two-tailed  $t$  tests. Differences between more than two groups were assessed by using one-way ANOVA. To compare the interaction between two factors, two-way ANOVA tests were performed. Analysis of variance, assessed by Bonferroni's multiple-comparison test, was used when comparing more than two groups. R (R software version 2.9.0) was used for the calculation of mean lifespan and s.e.m., and GraphPad Prism 5 (GraphPad Software) was used for all other statistical analyses. All  $P$  values  $< 0.05$  were considered to be significant. \* $P \leq 0.05$ ; \*\* $P \leq 0.01$ ; \*\*\* $P \leq 0.001$  instead stated otherwise. All animal experiments were performed once. Animals that showed signs of severity, predefined by the animal authorization no. 2432 were euthanized. These animals, together with those who died spontaneously during the experiments, were excluded from the calculations. These criteria were established before starting the experiments. In **Figure 6d**, two outliers (control) not

following the normal distribution of the samples were removed, based on a Shapiro–Wilk normality test. For lifespan experiments in *C. elegans*, sample size was determined as previously<sup>56</sup>. For all other experiments, sample size was estimated based on the known variability of the assay. All experiments were done non-blinded.

55. Kamath, R.S., Martinez-Campos, M., Zipperlen, P., Fraser, A.G. & Ahringer, J. Effectiveness of specific RNA-mediated interference through ingested double-stranded RNA in *Caenorhabditis elegans*. *Genome Biol.* **2**, H0002 (2001).
56. Mouchiroud, L. *et al.* Pyruvate imbalance mediates metabolic reprogramming and mimics lifespan extension by dietary restriction in *Caenorhabditis elegans*. *Aging Cell* **10**, 39–54 (2011).
57. Mouchiroud, L. *et al.* The NAD<sup>+</sup>/sirtuin pathway modulates longevity through activation of mitochondrial UPR and FOXO signaling. *Cell* **154**, 430–441 (2013).
58. Houtkooper, R.H. *et al.* Mitonuclear protein imbalance as a conserved longevity mechanism. *Nature* **497**, 451–457 (2013).
59. Frezza, C., Cipolat, S. & Scorrano, L. Organelle isolation: functional mitochondria from mouse liver, muscle and cultured fibroblasts. *Nat. Protoc.* **2**, 287–295 (2007).
60. Bratic, I., Hench, J. & Trifunovic, A. *Caenorhabditis elegans* as a model system for mtDNA replication defects. *Methods* **51**, 437–443 (2010).
61. Jha, P., Wang, X. & Auwerx, J. Analysis of mitochondrial respiratory chain supercomplexes using blue native polyacrylamide gel electrophoresis (BN-PAGE). *Curr. Protoc. Mouse Biol.* **6**, 1–14 (2016).
62. Vidal, K., Grosjean, I., evillard, J.P., Gespach, C. & Kaiserlian, D. immortalization of mouse intestinal epithelial cells by the SV40-large T gene. Phenotypic and immune characterization of the MODE-K cell line. *J. Immunol. Methods* **166**, 63–73 (1993).
63. Yamamoto, H. *et al.* NCoR1 is a conserved physiological modulator of muscle mass and oxidative function. *Cell* **147**, 827–839 (2011).